

UNIVERSITY OF AMSTERDAM

MSc Chemistry
Molecular Simulation and Photonics

Literature Thesis

A proposed Pathway for the Creation of a Ground State RbSr Molecule

Using Feshbach resonances and Stimulated Raman Adiabatic Passage with a Mott Insulator state as starting point

---

by
Marloes H.
Bistervels
10262806

February 2018

12 EC
October 2017-February 2018

Supervisor/Examiner:
Prof. Dr. Florian E. Schreck

Examiner:
Dr. Robert J.C. Spreeuw



Van der Waals-Zeeman Instituut

Contents

1 Abstract **3**

2 Introduction **4**

3 Theory **6**

3.1 The ultracold regime 6

3.2 Energy states of a system 7

3.3 Properties of Sr, Rb and RbSr 9

4 The Mott Insulator State **11**

4.1 A Mott insulator state 11

4.2 Bose-Hubbard model 11

4.3 A dual Mott insulator state 13

4.4 A Mott insulator state for RbSr 13

5 Feshbach resonances **15**

5.1 Theory of Feshbach resonances 16

5.2 Experimental procedure of Feshbach resonances 20

5.3 Feshbach resonances in RbSr 22

6 Stimulated Raman Adiabatic Passage **27**

6.1 Theory STIRAP 28

6.2 Experimental procedure of STIRAP 29

6.3 STIRAP scheme for RbSr 32

7 Summary and Outlook **40**

7.1 Summary 40

7.2 Outlook 41

8 Acknowledge **42**

1 Abstract

Ground state molecules are molecules with only their lowest energy levels occupied, hence they can be considered as ultracold. The well-defined states of those molecules allow us to have a high control over them. This is useful for the examination of quantum mechanical systems and for applications that need high sensitivity and accuracy. Production of molecules with polar and magnetic moments in their ground states bring along additional parameters that can be controlled. These additional controllable parameters are promising for new quantum devices, such as quantum computers and new quantum matter, but as well as for the understanding of many-body systems at the quantum mechanical level. The rubidiumstrontium (RbSr) molecule is one of those molecules with an electron spin and a large electronic dipole moment in the ro-vibrational ground state, and is seen as an anticipated molecule to investigate matter with topological order and to examine strongly correlated quantum phenomena. In this literature thesis the proposed pathway to achieve an ultracold RbSr molecule in the ro-vibrational ground state out of a Bose-Einstein Condensate (BEC) of Rb atoms and a BEC/Degenerate Fermi Gas (DFG) of Sr atoms is discussed. A Mott insulator (MI) state reduces loss of efficiency due to inelastic collisions and maintains the well-defined states of the atoms and produced molecules. An optical lattice mixture of ^{84}Sr-^{87}Rb have been obtained by the group of Schreck. Feshbach resonances (FRs) are used to produce weakly-bound RbSr molecules. These FRs have been recently observed by Barbé s*et al.* and can be invoked by three coupling mechanisms. The Stimulated Raman Adiabatic Passage (STIRAP) method is supposed to bring a weakly-bound RbSr molecule to the ground state by a coherent two-photon transition. Theoretical research by Chen *et al.* finds STIRAP schemes with an efficiency of 60% using an intermediate state ($|2(\Omega = 1/2), v' = 21, J' = 1\rangle$). Pototschnig *et al.* found a STIRAP scheme through the $1^2\Pi \leftarrow X^2\Sigma$ to be the most promising. A model representing the complete spectrum of the X$(1)^2\Sigma^+$ ground state of RbSr has been obtained by the group of Schreck by combining spectroscopic data of hot and ultracold RbSr in their analysis and is promising to guide future experiments.

2 Introduction

In the ultracold regime, atoms have almost zero kinetic energy and occupy their lowest energy states. This almost motionless state of ultracold atoms leads to long-lived and well-defined quantum states for each of their degrees of freedom. These properties allow the system to be highly controlled in the laboratory providing states with a long coherence time that are perfect to examine quantum mechanical principles [5] [25]. By converting this understanding into manipulation, cold atoms can be used for numerous applications such as high precision measurement, accurate atomic clocks, and very sensitive atom sensors [174] [15] [92].

The production of ultracold molecules has gained an increasing interest and activity in research after the achievement of ultracold atoms in the ground state. The production of a ground state bosonic atom gas, a so called Bose Einstein Condensate (BEC) [41] [3], was followed by a ground state fermionic atom gas, a Degenerate Fermi Gas (DFG), some years later [45]. Being an important challenge, researchers have attempted to produce ultracold molecules since the year 2000. The first cold molecules were, due to their ease of cooling, systems of alkali (AK) or alkaline-earth (AKE) homo-dimers [49] [76] [53] [167] [133] [36] [86] [147] [105] [38] [40]. For heteronuclear molecules with a closed shell containing AK and AKE earth atoms extensive research was carried out by several groups [166] [70] [87] [180]. In 2008 several groups reported formation of ultracold gases of polar molecules in the molecular ground state: LiCs reported by Deiglmayr *et al.* [43], Cs_2 reported by Danzl *et al.* [38], Rb_2 reported by Lang *et al.* [105], and KRb reported by Ni *et al.* [120]. The fermionic KRb molecule recently reached quantum degeneracy [117] [33].

Recently, efforts are carried out in the achievement of new systems of polar quantum gases with additional long-range interactions in the ultracold regime [51] [34] [116]. Systems with long-range interactions can be found in AK-AKE heteronuclear molecules. The long-range interaction can be seen due to the permanent or instantaneous dipole moments that are inhomogeneities of their charge distributions arising from the one unpaired electron in the ground state [106] [99].

The rich internal structure of molecules are seen to allow promising novelties in new applications as quantum-information devices and extremely high precision measurement [98] [23] [8]. The magnetic dipole enables these systems to be encoded and give an additional set of interactions within the system as well as with external fields [68] [75]. Furthermore, the anisotropic effect of the dipole moment in AK-AKE molecules enables the investigation of matter with topological order and strongly correlated quantum phenomena [111] [34]. This can also be useful in quantum simulation of lattice models [28] [16], control of chemical reactions [42], and novel forms of quantum matter [94] [102] [168]. RbSr is seen as a good candidate with many prospects due to its electron spin and large electronic dipole moment in the rovibrational ground state [72]. Besides that, the atoms Rb and Sr are extensively examined and used in the ultracold regime [6] [124].

Two main pathways to bring molecules into the ultracold regime are known. The first is the direct pathway which associates the atoms, and then cools the molecule to the lower temperature regime. Methods used for the cooling of atoms, such as Doppler cooling [126],

buffer gas cooling [50] [79] [136] [93] [163], Stark deceleration [14], and Sisyphus cooling [79], cannot be used with the same efficiency for molecules in the direct pathway due to the rich internal structure of molecules [176] [4].

The second is the indirect pathway which first cools down the atoms to the ultracold regime, and then assembles them into molecules [23]. This indirect pathway provides full control over the quantum state, because it can be initialized precisely, and the interaction between the atom pair can be controlled [76]. Techniques used for molecule association are photoassociation [44] [91] [131] [88], Feshbach resonances (FRs) [87] [76] [25] [95], and Stimulated Raman Adiabatic Passage (STIRAP) [11] or combinations thereof. The combination of FRs and STIRAP is the most common way to achieve ultracold molecules nowadays. The FR creates a weakly-bound Feshbach molecule out of a two-atom scattering state [159] [156] [112]. This Feshbach molecule is in a bound state that is too weak to have a dipole moment. By using STIRAP the weakly-bound molecule can be transferred to the ro-vibrational ground state [161] [162] [170] [175]. For polar molecules, this pathway is the only known way to their ro-vibrational ground states [116]. Some examples include fermionic $^{40}K^{87}Rb$ [120], bosonic $^{133}Cs_2$ [39], bosonic $^{87}Rb^{133}Cs$ [114], fermionic $^{23}Na^{40}K$ [123], and bosonic $^{23}Na^{87}Rb$ [73].

The extension of the application of the Feshbach-STIRAP pathway to an AK-AKE molecule, like RbSr, emerged after Hutson, Aldegunde and Zuchowski in 2010 showed theoretically that a Feshbach resonance also could occur for RbSr [177]. Sophisticated atom-traps created a basis for the development of applications as well as extension to more complex molecules with higher efficiency [71] [152] [26]. Experimental attempts to obtain ground state closed shell alkali-metal-Yb were done for YbRb [140] [119], YbLi [121] [81] [173] [135], and CsYb [74]. YbRb was obtained in the electronic ground state by two-color photoassociation and appeared to be challenging due to unfavorable scattering properties [17]. YbLi has its exciting prospects but so far no ground state molecules have been obtained. Experimentally, the Schreck strontium quantum gas group reported a quantum degenerate mixture of $^{84}Sr^{87}Rb$ atoms in 2013 [124]. Recently, weakly-bound bosonic $^{88}Sr^{87}Rb$ molecules and fermionic $^{87}Sr^{87}Rb$ molecules have been observed for the first time by this group [9].

In this report the proposed pathway to achieve ultracold RbSr molecules in the ro-vibrational ground state out of a Rb atom from a BEC and a Sr atom from a BEC or DFG will be discussed. The report starts with a brief description of the fundamentals of atoms in the ultracold regime, energy levels and properties of the Rb and Sr atoms, and RbSr molecules. This will be followed by the explanantion of the pathway that has been proposed to obtain a ground state RbSr molecule. This pathway consist of three steps: A Mott insulator (MI) state of two ultracold atoms as starting point, followed by the process of magnetoassociation using FRs, and finally the STIRAP method. The general concept will be outlined for each step, and each section will conclude with its application for the production of ground state RbSr molecules.

3 Theory

This chapter provides background information on atoms and molecules in the ultracold regime. The chapter starts with the description of the structure of a single atom and its behavior in the ultracold regime. This will be followed by a short recap of energy levels and states. The chapter with the basic characteristics of Rb, Sr, and RbSr.

3.1 The ultracold regime

The thermal de Broglie wavelength

Louis de Broglie suggested that matter exhibits wave-like behavior which follows the standard quantum mechanical postulates. He stated that the corresponding wavelength of a particle, the de Broglie wavelength (λ_{db}), was proportional to the inverse of the momentum of the particle, which gives the de Broglie relation [7],

$$\lambda_{db} = \frac{h}{p}, \tag{1}$$

where h is Planck's constant and p the momentum of a particle. The average wavelength of particles in an ideal gas at a specified temperature, the thermal de Broglie wavelength (λ_{th}), is obtained by substitution of the momentum by the kinetic energy [7],

$$\lambda_{th} = \sqrt{\frac{h^2}{2\pi m k_b T}} \tag{2}$$

where the momentum can be expressed by the kinetic energy as $p = \sqrt{2mE_{kin}}$. In the non-relativistic case, the average thermal energy of a free particle is $E_{kin} = \pi k_b T$ [7].

Quantum degeneracy

When the thermal de Broglie wavelength is similar or larger than the inter-particle spacing as shown in figure 2, the system cannot be described classically anymore [139]. In this case quantum degeneracy occurs and the system has to be described by quantum mechanical principles. Applying this conditions on 2 with the Bohr radius a_0 as λ_{th} leads to temperatures of at least 100 nK in the ultracold regime [7].

A degenerate quantum gas particle occupies the levels of the confining trap according to quantum statistics [132]. If bosonic or fermionic quantum statistics has to be used is governed by the total spin of the atom, which is a combination of proton, electron, and neutron spin, all of which are fermions. Hence, if the total number of electrons, protons and neutrons is odd we have a fermion. Two fermionic or two bosonic particles can pair up to form a composite boson. A combination of a fermionic and a bosonic particle will end up as a composite fermion [95]. If the particle is bosonic then Bose-Einstein statistics are followed and a BEC is obtained at the moment that all the particles of the gas are occupying the same ground state as is shown in panel (a) of figure 1 [55]. If the particle is fermionic then the Fermi-Dirac statistics are followed and a DFG is obtained at the

moment that all particles occupy the lowest energy states as possible as is shown in panel (b) in figure 1 [47].

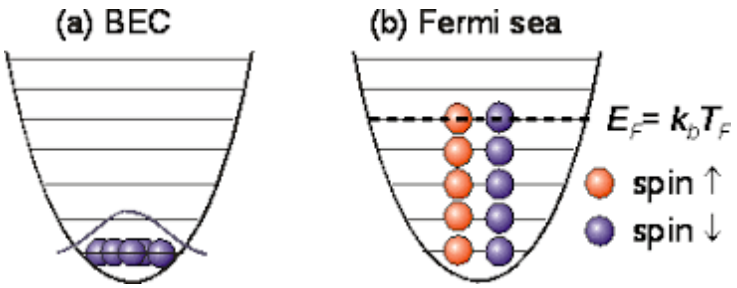


Figure 1: Quantum statistics for bosonic and fermionic particles in a potential well. (a) BEC for bosonic particles and (b) DFG for fermions or fermionic particles, all states up to the Fermi energy E_F are occupied. Figure is copied from [132].

Besides a low temperature, BECs and DFGs require low entropy and high phase-space density [120]. The phase-space can be pictured by considering all the states of a system that are existing in a n-dimensional space. The phase-space density (PSD) is the number of states per element of volume in phase-space. At a value of approximately PSD = 1, a transition in phase-space will occur to a BEC for bosons and and DFG for fermions [120] [65]. The critical point at which one speaks about a BEC can be calculated by the PSD [158],

$$PSD = n_{pk}\lambda_{db}^3, \tag{3}$$

where n_{pk} is the peak number density of the sample and λ_{db} is the wavelength of the particle. n_{pk} can also be written as N/V, where N is the number of atoms and V is the volume of the atomic cloud [158].

3.2 Energy states of a system

The stationary Schrödinger Equation

The energy levels of a quantum state subjected to an Hamiltonian H can be obtained by using the stationary Schrödinger Equation (SE) [7],

$$\hat{H}\Psi(r) = E\Psi(r) \tag{4}$$

where wavefunction $\Psi(r)$ and energy E are an eigenstate and corresponding eigenvalue of the stationary SE respectively. $\Psi(r)$ describes the system with regard to its position and momentum. E represents the energy of the corresponding wavefunction. $\hat{H}$ can be expressed in a kinetic and a potential part [7],

$$\hat{H} = -\frac{\hbar^2}{2M}\nabla^2 + V(r), \tag{5}$$

where $-\frac{\hbar^2}{2M}\nabla^2$ represents the kinetic energy, with M the mass of the system. $V(r)$ describes the effective potential [7].

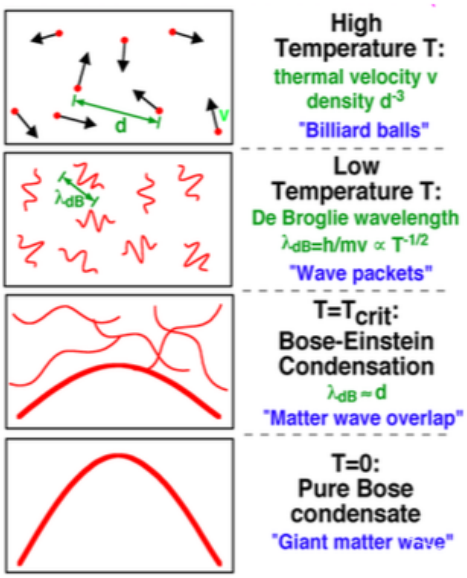


Figure 2: The de Broglie wavelength and interparticle distances at different temperatures for bosons. At zero T, the particle can be described by one giant matter wave. Figure is copied from [41].

In case of a many-body system the Hamiltion subjected to the system, see equation 4, includes an extra term to include to interaction between the different particles. In this case the potential becomes [25]

$$V_\ell(r) = V(r) + \frac{\hbar^2 \ell(\ell+1)}{2Mr^2}, \tag{6}$$

where ℓ is the angular momentum and M is the reduced mass of the system [25].

Atomic spectra splitting

Additional effects lead to a splitting of the calculated energy levels. These effects are divided in three types: a fine-structure, such as spin-orbit coupling and other relativistic effects, hyperfine structure, such as the coupling of nuclear and electron magnetic moments, and effects from external electromagnetic fields, such as the Zeeman or Stark effect [7]. Because the transitions between hyperfine states have extremely small energy differences, the states are very stable and have a long lifetime, which makes them useful in high precision measurement [34].

A hyperfine structure can be found for a nucleus that has spin but also for a quadrupole moment of a nucleus with an electric-field gradient.

The nuclear spin i, can couple with the total electronic angular momentum j, with $\mid \ell - s \mid < j < s + \ell$ [25] [95]. This coupling results into the total angular momentum f in the range of $\mid i - j \mid < f < i + j$. The total angular momentum gives rise to the hyperfine splitting of the energy states. The magnetic field, B, splits the f state into $2f + 1$ sublevels, m_f, as shown in figure 3. The value of m_f ranges from $-f, \ldots, 0, \ldots, f$,

and the corresponding levels have energy differences proportional to the applied magnetic field [25] [95]. Therefore f only maintains its value at $B = 0$. At $B \neq 0$, f cannot be seen as a good quantum number anymore, whereas m_f can [177]. This leads to the conservation law of m_f [25] [95]. Molecules their energy levels are characterized by the total angular momentum f by $F = \sum_i f$, and the conservation of m_f still holds by $M_f = \sum_i m_f$ [78].

The dependence on the magnetic and electric fields is well-known as the Zeeman-effect and Stark-effect respectively [95]. The Breit-Rabi formula can be used to approximate the energy states $|f, m_f\rangle$ in a magnetic field [20].

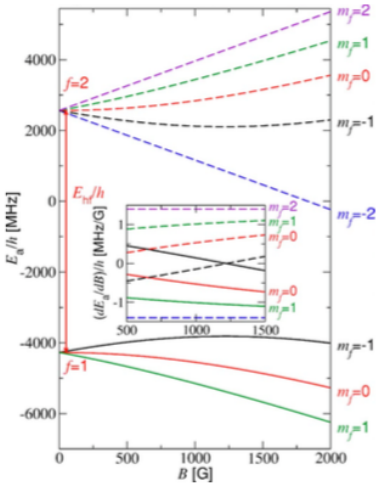


Figure 3: The hyperfine states energies of a ^{87}Rb atom in its $5^2S_{1/2}$ state in dependence of an applied magnetic field, calculated by the Breit-Rabi formula. In the inset, $\delta E/\delta B$ is plotted over the applied magnetic field. Figure is copied from [95].

3.3 Properties of Sr, Rb and RbSr

Strontium

Strontium atoms have been well-studied in the ultracold regime. A BEC of the ^{84}Sr isotope was obtained by Stellmer *et al.* in 2009 [145]. Sr allows us to explore a diverse range of experiments due to its rich electronic structure. The electronic structure configuration is [Kr]$5s^2$. Because of the two paired electrons in the outer shell, Sr has a singlet ground state that gives rise to a $^1S_0$ term [7]. Excited states can be singlet states for antisymmetric spin states or triplet states for parallel spin states. The atom has different stable isotopes, including three bosonic isotopes, ^{84}Sr, ^{86}Sr, ^{88}Sr, and a single fermionic isotope ^{87}Sr with nuclear spin $i = 9/2$. Very reactive unstable isotopes are ^{89}Sr and ^{90}Sr [143].

The nuclear spin and charge distribution causes level splitting of the electronic states. The fine structure involves energies of transitions that fall within the visible light spectrum [143]. Coupling with an electric field such as light, the AC Stark shift, leads to a tunable shift in the energy states with a dependency of the intensity and frequency of light. This AC Stark shift is used to tune energy levels and transition frequencies [19] [143]. Only the

^{87}Sr isotope also has a hyperfine splitting due to its $i = 9/2$ nuclear spin. The hyperfine structure of the electronic levels of the fermionic ^{87}Sr is found to be of the order of 10 MHz to 1 GHz [143].

Rubidium

Rubidium was the first atom with which a BEC was created [3] and is used is many ultracold experiments. The electron configuration is [Kr]$5s^1$, corresponding to the single ground state term $^2S_{1/2}$ [7]. Excited states are doublet states. The atom has a natural abundance of two isotopes; one stable ^{85}Rb, and one effectively stable ^{87}Rb [141].

A hyperfine structure arises in both of the isotopes due to a magnetic spin. The total nuclear momentum of ^{87}Rb is $i = 3/2$ and its hyperfine levels are $f = 1$ and $f = 2$. ^{85}Rb has a total nuclear momentum of $i = 5/2$ and therefore hyperfine levels are $f = 2$ and $f = 3$. The hyperfine structure splitting of the Rb atom needs very precise laser pulses. Values of the hyperfine structure splitting can be found on the order of a few 100 MHz [141].

The RbSr molecule

RbSr is a paramagnetic and polar molecule. Ground state RbSr is an anticipated molecule for many applications as RbSr possesses both a magnetic and an electric dipole moment in its ground state. The electronic ro-vibrational ground state is composed by Rb ($^5s^1$, $^2S_{1/2}$) + $Sr(^5s^2, {}^1S_0)$ and has the molecular term symbol $^2\Sigma^+$ [7]. The ground state has a doublet spin configuration that arises from the unpaired electron in its outer valence shell [178]. A permanent electric dipole moment of RbSr in its lowest configurational state is found to be $1.4 - 1.5$ D [72] [67]. The total angular momentum's projection onto the magnetic axis of the RbSr molecule is described by the Rb atom, because the presence of the Sr atom has almost no effect on the hyperfine state of the Rb atom. The values of M_f, where $M_f = m_{Rb} + m_{Sr} + m_\ell$, lie almost parallel to the Rb atomic states as a function of magnetic field [9]. These characteristics enable the manipulation of a ground state RbSr by both external magnetic and electric fields.

The electronic first excited states of RbSr correspond to $s \rightarrow p$ transitions in Sr or Rb in the dissociation limit. The subsequent relevant excited states of RbSr are the doublet and quartet states of Σ, Π and Δ [130]. Excitation in Rb leads to a ^2P $(5p)$ state [178]. Excitation in the Sr atom leads a $^3P_{0,1,2}$ or ^1P $(5s5p)$ state [24]. Excited states are commonly denoted in alphabetic order in front of the molecular state term [7].

If the spin-orbit (SO) coupling is included, states are distinguished by Ω. Ω arises from the sum of the total spin S and the molecular angular momentum Λ and represents the projection of the total angular momentum along the internuclear axis [7].The values of Ω in RbSr of the lowest asymptotes are 1/2, 2/3 an 5/2 [178].

Characteristic properties can be derived from the PECs for the ground and the lowest excited electronic potentials of RbSr and will be discussed in the theoretical calculation for setting up a STIRAP scheme.

4 The Mott Insulator State

In this chapter, the Mott insulator state is explained with the Bose-Hubbard model, followed by a discussion of the dual Mott insulator state. The chapter closes with the application of an MI state for RbSr molecules.

4.1 A Mott insulator state

The proposed pathway of association of ultracold Sr and Rb atoms into an ultracold quantum gas of RbSr makes use of an MI state as starting point. The MI state can be seen as a crystalline solid state, where the arrangement of the particles is obtained due to the confinement of an optical lattice [69]. An optical lattice is a periodic standing wave potential created by back reflected laser beams far off resonant from any atomic transition as shown in figure 4 [84]. By controlling the frequency and intensity of the laser the number of atoms can be determined per lattice site. In an MI state, atoms are localized with an occupation of n atoms per lattice sites [69]. This is opposite to a superfluid (SF) that is a fluid state with zero viscosity.

The use of an MI state in the formation of ground state molecules brings several advantages along and was first suggested by Jaksch *et al.* [83]. First of all, the MI state leads to an increase in lifetime and can overcome challenges of chemical reactivity [176]. The loss rate due to elastic and inelastic collisions and tunneling is highly reduced [34] [144]. Secondly, the tight confinement ensures the initial state of atom pairs being well-defined. The pinned particles in an optical lattice enable the study of correlation effects and the long-range nature of dipole-dipole interaction in a clean manner [116].

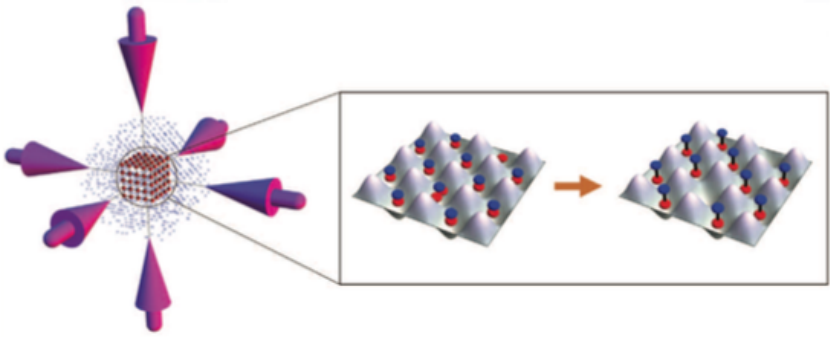


Figure 4: A dual Mott insulator state created by a 3D optical lattice. The red particles are loaded in excess (left lattice). The sites occupied with one particle of each species have the highest probability to produce molecules (right lattice). Figure is copied from [117].

4.2 Bose-Hubbard model

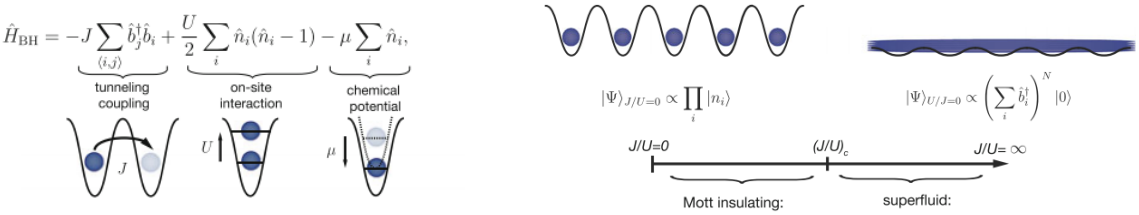
The transition to an MI state from a SF state is driven by tuning the potential of the optical lattice, which can be described and predicted by the Bose-Hubbard model (BHM)

[69] [82]. The BHM is a Hamiltonian consisting of three terms: a tunneling term, a mean-field shift and an external potential [62],

$$\hat{H}_{BHM} = -J \sum_{<i,j>} \hat{a}_i^\dagger \hat{a}_j + \frac{1}{2} U \sum_i \hat{n}_i(\hat{n}_i - 1) + \sum_i \epsilon_i \hat{n}_i. \tag{7}$$

The tunneling part describes the hopping energy that is related to the kinetic energy, where J is the tunnel/hopping matrix element, i and j are particle that are nearest neighbours, $\hat{a}_i^\dagger$ is the creation operator that creates a particle at site i, and $\hat{a}_j$ is the annihilation operater that destroys a particle at site j. The mean field-shift is caused due to pairing of particles, where U is the on-site interaction parameter, $\hat{n}_i$ is the number density, and ϵ_i is the external potential energy [69].

The parameters J and U are important properties defining the physics of the system. In solid state crystal these parameters are defined by the system itself, whereas in ultracold atom systems these parameters can be easily tuned over a large range by modifying the confining potential. Weak laser intensities lead to a shallow lattice where J is big and U is small, whereas strong lasers create a deep lattice in which J is small and U is big. Ramping on or off the laser frequency can increase or decrease the atom density at the lattice site. Raising the potential too high leads to a loss of phase coherence [115] [179].



(a) (b)

Figure 5: The Bose-Hubbard model. (a) Upper picture describes the physical situation per term in the $\hat{H}_{BHM}$. (b) The figures show the particle distribution for an MI state (left) and a SF state (right). Figures are copied from [56].

Limits of Bose-Hubbard model

Considering the limit where $U/J \gg 1$, the onsite interaction energy is way larger than the kinetic energy that it costs to hop between lattice sites. The system is in a strongly interacting regime [69]. Starting from a system with one atom per site, every hopping event results in a pair of atoms, which increases the total energy of the system. Hence, pairing by hopping is disfavored which results in a lack of mobility. In this regime an MI state will be obtained by N sites occupied by n atoms as shown in panel (b) in figure 5. The corresponding wave function with exactly n atoms per site can be described by [56]

$$|\Psi_{MI}\rangle \propto \prod_{i=1}^{N} \left(\hat{a}_j^\dagger\right)^n |0\rangle \,. \tag{8}$$

When $U/J \ll 1$, the kinetic energy is way larger than the onsite interaction energy. The system is in a weakly-interacting regime [69]. Hopping that leads to pairing is favored as it effectively lowers the total energy and a superfluid phase will be obtained with an Poisson distribution [56],

$$|\Psi_{SF}\rangle \propto \left(\sum_{i=1}^{N} \hat{a}_j^\dagger\right)^n |0\rangle \,. \tag{9}$$

4.3 A dual Mott insulator state

Two different MI states can be combined in the same optical lattice to obtain a dual MI state. Here two atomic species are considered to both occupy every site of the optical lattice as shown in figure 4. The density overlap, describing the site occupations of the two species in the potential well, complicates the achievement of the dual MI state, since the individual species can have different requirements [116] [149]. Interspecies repulsion and different gravitational sag are main reasons for spatial separation of the ultracold mixture [10]. The immiscibility parameter Δ compares the intraspecies and interspecies interactions [10],

$$\Delta = g_1 g_2 / g_{12} \tag{10}$$

where $g_i = 4\pi\hbar^2 a_i/m_i$ and $g_{12} = 4\pi\hbar^2 a_{12}/m_{12}$ with a_i and a_{12} being intraspecies and interspecies scatterlength respectively and m_i and m_{12} the atomic and reduced mass respectively. Mixtures with values of $\Delta < 1$ turn out to be immiscible [10].

Differences in gravitational sag can be due to difference in polarizability or difference in masses that leads to an experience of different trap potentials or a different gravitational force respectively [10]. An optimization in density overlap of the two species is created by considering of the overall potential landscape, geometry and atom numbers of species during the loading [10]. For a high efficiency in the molecule formation the initial atom numbers must be maximized, as only double occupied sites will contribute in the molecule formation. After a dual MI loading, the lattice depth should be increased to suppress tunneling and the frequency can be moved further away from atomic or molecular resonance to reduce interactions, preserving the mixed dual state [115].

4.4 A Mott insulator state for RbSr

Lattice mixture

RbSr is not stable, with a collision the chemical reaction $2\mathrm{RbSr} \rightarrow \mathrm{Rb}_2 + \mathrm{Sr}_2$ occurs on a fast time scale. Therefore a dual MI with sites where the population is characterized by one Rb and one Sr atom in the ground state would be desirable [10]. Up to now, lattice mixture is only done for ^{84}Sr-^{87}Rb, which was shown to have a Δ value of 1.3 [10]. Values for interspecies s-wave scattering lengths for different isotopic species of Sr and Rb have been published by Ciamei *et al.* recently [27].

Gravitational sag for ^{84}Sr-^{87}Rb is caused by differences in polarizability. Rb has a higher polarizability than Sr, therefore Sr is weaker confined in an optical potential trap. The gravitational force is similar for both species, but due to the polarizability differences the vertical trap oscillation frequency is not the same. This causes a separation between

the two species. The group of Schreck used a bichromatic trap for ^{84}Sr-^{87}Rb, consisting of two overlayed far-detuned dipole traps to overcome this [10]. The first trap serves to create an attractive potential for both species. The second trap serves to tune the trapping frequencies for the two species independently. Due to a different dependency on the second extra trap, the gravitational sag can be balanced and a significant overlap has been obtained [10]. Another approached used by the group of Schreck is the combination of optical and magnetic trapping, earlier seen in reference [153]. But with the use of a magnetic gradient only a small overlap has been achieved between the BECs [10].

After the obtained overlap the double BECs have to be transferred to an optical lattice. This has been done in three subsecutive ramps. After the first ramp the Rb atoms are in the MI phase. After the second ramp the Sr atoms are in the MI phase. Finally the third ramp increases the lattice depth to bring both species deep in the MI regime [10]. The obtained state can be used as an ideal starting point for magnetoassociation or STIRAP, which will be discussed in the next chapters.

Quantum degenerate mixture generation

Another starting point for the association of ground state molecules is quantum degenerate mixture generation (QDMG). With this method ^{84}Sr-^{87}Rb and ^{88}Sr-^{87}Rb double BEC samples are obtained with low atom numbers with a temperature of 70 nK and 190 nK respectively [124]. For ^{88}Sr, a lower BEC atom number is obtained due to the negative scattering length that leads to a collapse of the BEC for the higher atom numbers [124]. For a Bose-Fermi mixture of ^{87}Sr^{87}Rb a quantum degenerate mixture would be extremely hard because of a large three-body decay rate.

In this method a storage trap, being a bulk trap, is first loaded with ultracold ^{87}Rb atoms. $^{84}/^{88}$Sr atoms trapped in a red magnetic-optical trap (MOT) are added with an excess of amount compared to the ^{87}Rb atoms. This results in a so called science dipole trap, a crossed beam dipole bulk trap. Here sympathetic cooling of the Rb atoms by the Sr atoms occurs [137]. Finally evaporative cooling is carried out to obtain a quantum degenerate mixture gas of the two BEC species [124].

In the case of the ^{84}Sr-^{87}Rb double BEC sample essentially a same scheme is used as in the case of ^{88}Sr-^{87}Rb double BEC. Two main difference of ^{84}Sr compared to^{88}S can be found in the scattering length and the natural abundance. The scattering lenght of ^{84}Sr is large and positive, $123a_0$, but the natural abundance of ^{84}Sr is very low compared to the ^{88}Sr. The lower natural abundance of ^{84}Sr can be compensated for by a longer blue MOT duration to obtain a same number of atoms accumulated as in the case of ^{88}Sr. The large and positive scattering length is well-suited for evaporative cooling. To optimize the QDMG scheme for ^{84}Sr-^{87}Rb both species, ^{84}Sr as well as ^{88}Sr, are used. One isotope after the other is loaded accumulated in the a metastable reservoir to which the laser frequency is changed according to the species loaded. The ^{88}Sr is used as refrigerant in the sympathetic laser cooling of Rb, whereas ^{84}Sr is used in the evaporative stage to end up with a ^{84}Sr-^{87}Rb double BEC sample. The ^{88}Sr have to be expelled by adiabatically lowering of the science trap before loading the ^{84}Sr, because their very large scattering length of $1700a_0$ would lead to a strong three-body decay [124]. Experimental details for DQMG an be found in reference [124].

5 Feshbach resonances

This chapter discusses the FRs used in RbSr. After a historical overview, the chapter continues with a theoretical part of FRs, including properties and coupling mechanisms of states involved in FRs, the scattering length and a picture of the total interacting system. This is followed with experimental aspects of the method. The chapter closes with a discussion of FRs and the associated coupling mechanisms of RbSr.

Feshbach resonances (FRs) are extensively used in ultracold atomic gases as a gateway with great control for ultracold molecule formation. As illustrated in figure 6, a FR is achieved when a scattering state can couple to a molecular bound state [95]. The resonance is caused by tuning the energies of the two states close to each other with the help of external parameters such as a magnetic or an electric field. At resonance a strong mixed state exist, in which the system can be described by a superposition consisting of the scattering state and the molecular bound state with universal properties [95].

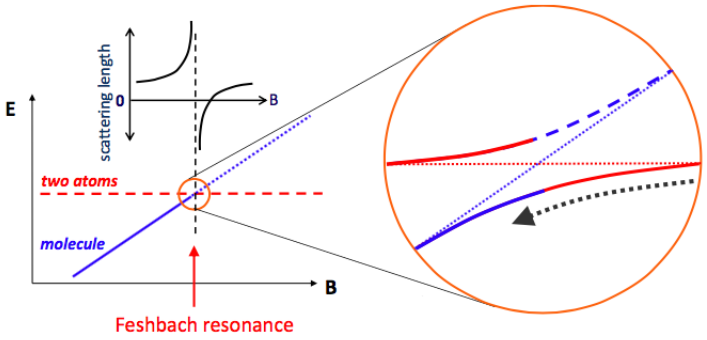


Figure 6: The energies of the scattering state (the dotted line) and the molecular state (the solid line) are plotted against the magnetic field. At the resonance point, where the two energy lines cross, the scattering length diverges and is a universal for the mixed state, pictured in the small diagram above the crossing point. In the enlargement, the avoided crossing due to coupling is shown. Figure is copied from [59] in [98].

For a decade, Feshbach resonance have been started to be used in the formation of heteronuclear molecules. First of them were $^{40}K^{87}Rb$ [120] and $^{6}Li^{40}K$ [46]. With improving detection technologies and more theoretical research, opportunities in the formation of molecules via Feshbach resonances have been revealed for a wide range of molecules [177] [21] [22] [1]. Optical methods have become accessible when the absence of magnetic moments prevents the use of magnetic FRs [88]. Marcelis *et al.* combined magnetic and optical detuning to obtain more control [107]. Even molecules with a single spin configuration in the ground state and very narrow linewidth, $\Delta \ll 1G$, are found to form a Feshbach molecule [9]. Nowadays the use of Feshbach resonances can now be considered an indispensable tool in current cooling pathways to obtain ultracold molecules. An extensive review of developments in Feshbach resonances can be found in reference [25].

5.1 Theory of Feshbach resonances

The two-body collision channel

To make FRs and the states involved more concrete, the FR can be described by a two-body collision channel picture as illustrated in figure 7. In the ultracold regime a collision channel can be represented by a potential energy curve (PEC) of the system. A collision channel, from now on referred to as channel, is defined by the energy curve in which atoms with a certain state can have interactions [95] [25]. Therefore the channel is described by the internal states q of the involved particles and the partial wave functions ℓ and m_ℓ [25] [110]. In the ultracold regime the this state q strongly depends on the energy of the Zeeman levels, and the configuration is defined by the Zeeman configuration leading to $q_i = f_i m_i$ [25]. An open channel corresponds with the PEC of the scattering state that has an energy E_g. A closed channel corresponds with the molecular state, which is a metastable vibrational state that exists in a certain energy range near the threshold of other states [95]. In the literature, this molecular state is often assigned to the Feshbach resonance state [25].

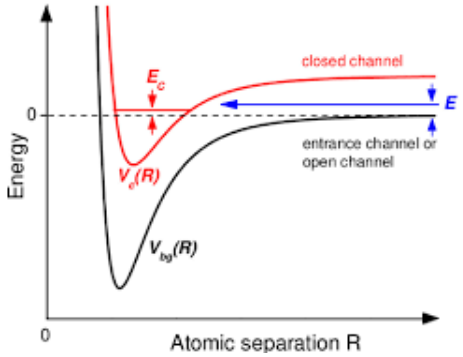


Figure 7: The open and closed channel potentials involved in a FR process. The dotted line presents the dissociation threshold of which the energy coincides with two separated atoms. The difference in energy between a weakly-bound state and the dissociation treshold is denoted with arrows. Coupling occurs due to resonance of the two-energy states. Figure is copied from [25].

The general two-body Hamiltonian

The total interacting system for the closed and open channel can be described by a general two-body Hamiltonian. This general two-body Hamiltionan is associated with the relative motion of an atom pair that depends on the internuclear distance r and the asscociated radial wave function and can be given by the matrix [25] [154] [95]

$$\hat{H}_{2body} = \begin{pmatrix} \hat{H}_g & W(r) \\ W(r) & \hat{H}_e(B) \end{pmatrix}, \tag{11}$$

where $\hat{H}_g = -\frac{\hbar^2}{m}\nabla^2 + V_g(r)$ and $\hat{H}_e(r) = -\frac{\hbar^2}{m}\nabla^2 + V_e(B, r)$. The diagonal solutions of this Hamiltonian in a SE are associated with the energies of the ground and excited states in

absence of coupling respectively. $W(r)$ represents the interaction between the two states as a function of the distance between the atoms [95].

Due to a difference in magnetic moments, the two states are differently affected by an applied magnetic field. A magnetic-field strength dependence can be found in an overall shift of the excited state potential. The energy of the bound state in the closed channel relative to energy of the atoms in the scattering state is [95]

$$E_c = \delta\mu(B - B_0), \tag{12}$$

where $\delta\mu$ is the difference in magnetic moments between the states and B_0 is the resonance position. As a consequence of the coupling at the resonance, the two states, denoted by their spin configuration α and β, are lifted in energy [65] [95],

$$\begin{aligned} \hat{H}_g\Psi_\alpha + W(r)\Psi\beta &= E\Psi_\alpha \\ W(r)\Psi_\alpha + \hat{H}_e\Psi_\beta &= E\Psi_\beta. \end{aligned} \tag{13}$$

The energy degeneracy at the crossing of the two states vanishes and an avoided crossing is created. This avoided crossing enables the transition between the states as shown in figure 6.

The eigenstate of the interaction Hamiltonian, known as the dressed stationary state, is a superposition consisting of the scattering state and the molecular bound states with corresponding amplitudes. The binding energy of the dressed stationary state can be found to be [95]

$$E_b = \frac{\hbar^2}{2Ma^2(B)}, \tag{14}$$

where M is the reduced mass and $a(B)$ is the scattering length of the dressed stationary state, which will be explained in the next section.

Scattering length

FRs are such a powerful tool because they can be used to control the scattering length of an atom pair [59] in [98]. The scattering length a is proportional to the interaction between atoms in an atom pair and determines the collision rate of the interacting atoms. The value and sign of the scattering length gives an indication of the amount of attraction or repulsion energy between two atoms [25]. A large and positive scattering length means a strong repulsive potential, whereas a negative value indicates an attractive strength. At the singularity of a the value diverges to plus or minus infinity. At this point it can be said that two separated atoms are at the threshold of a bound state, which is often associated with the highest vibrational bound state in the open channel [25]

The scattering length depends on the interaction potential and on the reduced mass of the particles involved. Therefore, the value of a varies with the state and different isotopic species. According to the *Effective range theory* [13], in the limit of zero collision energy where k, the wavenumber, goes to zero, the scattering length can be seen as a hypothetical hard sphere radius where scattering occurs.

In principle a is only weakly-dependent on the value of B. This changes at the values of B that create degeneracy in energy of a scattering state and a resonance state leading

to the strong mixed state. This mixed state has universal properties that can be described by a [95] as is expressed in equation 14. The reason of the dependency of a on B lies in the difference between the magnetic moments of the states (μ). This dependency allows for the sign and magnitude of a to be tuned by B and enables manipulation and control of the collision rate [155]. As illustrated in figure 8, the dependence of a on the magnetic field can be expressed as [113]

$$a(B) = a_{bg}\left(1 - \frac{\Delta}{B - B_0}\right), \tag{15}$$

where a_{bg} is the scattering length of the scattering state for off resonant values, and B_0 represents the position of the singularity of the scattering length. At resonance B_0, the metastability of the resonance state causes a time delay in the collision that results in an enhancement of collisional cross-section. The zero crossing is at the position $B{=}B_0 + \Delta$ where $a(B)$ has a zero value. Δ is the resonance width, which is determined by the strength of the interaction, $W(r)$, of the two states using Fermi's Golden rule [118] [154],

$$\Delta(E) \propto 2\pi \mid \langle \Psi_{mol} \mid (W(r)) \mid \Psi_{scat} \rangle \mid^2 . \tag{16}$$

Equation 15 is only true for purely elastic scattering. If decay to lower energy channels is possible, a non-zero imaginary component has to be included in the equation. An explanation for this can be found in reference [77].

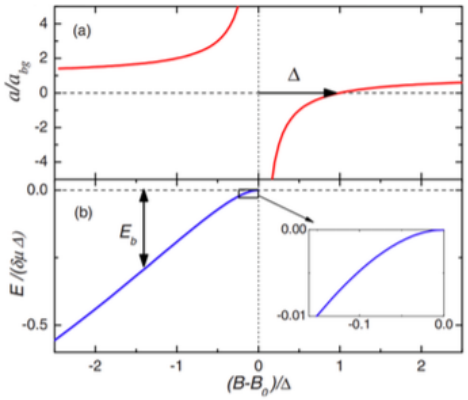


Figure 8: The upper panel shows the asymptotic behavior of the scattering length according to its deviation from its resonance position that is set to B=0. At this point the scattering length diverges from $-\infty$ to ∞. The resonance width Δ is defined by the zero crossing point and the resonance position. The lower panel shows the binding energy E_b that can be described by equation 14 at B_0, emphasized in the inset, but varies linearly with B further away from B_0 [25].

Coupling between states

Two channels become coupled when molecular levels of the channels are degenerate and a coupling mechanism $W(r)$ between the channels exist [95]. To determine the molecular

states that are coupled to the scattering state, common components have to be considered in $\langle q_1 q_2 \ell m_\ell | q_{mol} \ell m_\ell \rangle$. Collisions are, besides conservation of the symmetry of the total wave function, strictly restricted to the conservation of the quantum number $M = m_1 + m_2 + m_\ell$ [25]. Conservation of energy allows the atoms only to convert into states with lower energy than E_{tot}.

The molecular bound states are inferred from the recoupling of the atoms in the scattering state. Interactomic recoupling of the spin angular momenta results in the total angular spin, $S = s_1 + s_2$ of diatomic states. For example, two atoms with $s = 1/2$ give rise to a singlet or triplet molecular spin configuration, since the multiplicity is $2S + 1$ [95]. When the nuclear spin i also has a non zero value, more diatomic states have to be considered, since i can couple to j producing the hyperfine levels f as is explained in the theory chapter.

The possible bound and scattering states that can couple can be found by solutions of the SE with the general two-body Hamiltonian, given in equation 11. The associated radial wave function of the atoms in the scattering state can be expressed as a coupled-channel expansion in the separate atom spin basis [118],

$$|\Psi_\alpha(r, E)\rangle = \sum_\beta |\beta\rangle \, \psi_{\beta\alpha}(r, E)/r, \tag{17}$$

where the allowed states $|\beta\rangle$ are those that obey conservation of parity and of $M = m_1 + m_2 + m_\ell$, $\psi_{\beta\alpha}(r, E)/r$ is the radial wave function [25].

Substituting equation 17 into the SE (equation 4) in combination with imposed boundary conditions for the radial wave functions leads to the coupled equation [95],

$$\frac{\delta^2 \psi_\alpha(r, E)}{\delta r^2} + \frac{2M}{\hbar^2} \sum_\beta [E_{\delta\alpha\beta} - V_{\alpha\beta}(r)] \psi_\beta(r, E) = 0, \tag{18}$$

where the first terms represent the kinetic energy, and $E_{\delta\alpha\beta}$ is the total energy of a state with spin configuration α or β. $V_{\alpha\beta}(r)$ includes the potential energy of the state α as well as the interaction potential of inter-channel coupling. The interaction potential represents the coupling mechanism and determines the value of the coupling strength [95],

$$V_{\alpha\beta}(r) = [E_\alpha + \frac{\hbar^2 \ell(\ell + 1)}{2\mu r^2}] \delta_{\alpha\beta} + V_{\alpha\beta}^{int}, \tag{19}$$

where the interaction potential $V_{\alpha\beta}^{int}$ term consists of electronic Born-Oppenheimer potentials and relativistic electronic spin-dependent interaction potentials[25],

$$V_{\alpha\beta}^{int} = V_\ell + V_{ss}. \tag{20}$$

$V_\ell(r)$ represents the strong electronic interaction with only diagonal elements in ℓ. The total angular momentum of the diagonal elements is formed by a weighted sum of the Born-Oppenheimer potentials with the same spin value. Off-diagonal values in $\{f, m_f\}$ depend on the difference between $V_{S=0}$ and $V_{S=1}$. Therefore a coupling can be found in systems having a triplet and singlet spin state with the same ℓ [25] [37].

V_{ss} represents the weak relativistic spin-spin potential energy and second order spin-orbit interaction [25] [97] [146] [113]. This interaction arises from the anisotropic electron spin interaction and generates off-diagonal elements in both ℓ as well as in the hyperfine states $\{f, m_f\}$. Partial waves with different values of ℓ can be coupled, although it is restricted to $\Delta\ell = 0, \pm 2$.

The extension of the description of the system with spin character would indicate that the resonance is restricted to certain partial waves and the projection quantum number M_f. However, as will be later explained in the section on the coupling mechanisms of FRs in RbSr, resonances with coupling mechanisms beyond $\Delta M_f = 0$ have recently been observed [9] [1].

5.2 Experimental procedure of Feshbach resonances

Magnetic ramp

Most schemes to associate pairs of ultracold atoms into molecules rely on a magnetic field ramp across a FR. In these schemes, atoms are placed in a magnetic field B, in which $B > B_0$ and $a_{bg} < 0$ [156] [159] [112]. Then, the magnetic field is slowly ramped to $B < B_0$, causing a_{bg} to switch sign in an adiabatic evolution. This ramp of magnetic field is in agreement with going from the attractive side to the repulsive side of a scattering state [34]. An adiabatic evolution means that the change rate is so slow that the state vector has enough time to adjust to the system to maintain alignment with the eigenstate so that no transitions between the different states occur [30]. The eigenstate of the interacting system coincides initially only with the atom pair. In the region where B = B_0, we obtain a mixed state where the two states are so strongly coupled that universal properties hold. This means that one single effective molecular potential represents both states with one scattering length $a(B)$. In this region $a(B)$ is very large and positive and determines the binding energy, as can be derived from equation 14 and 15 [25] [95]. By ramping the magnetic field further the eigenstate coincides with the amplitude of the bound state. Here, further away from B_0, the binding energy varies linearly with B as is shown in figure 8 [25] [95].

Roughly speaking, in narrow resonances, with typically widths $\Delta \ll 1G$, the universal range exists only for a small fraction of the magnetic field. Because of this, the states have the spin character of the entrance channel only over a small fraction of the width. The FR must be modeled with a coupled channel picture in this case, and the adiabatic evolution is even more important to maintain aligment of the mixed state [34] [95]. In a broad resonances, with typically widths $\Delta \gg 1G$, the universal range exist over the entire fraction of the width and is easily modeled using the magnetically tunable scattering length represented by a single potential describing the mixed state [25]. The exact definition of the difference between narrow and broad resonances is more complicated and a discussion can be found in reference [151].

The ramp speed in the FR process is crucial for the efficiency of the molecule forma-

tion. Its dependency can be deduced from the Landau-Zener model that indicates the probability of atoms to be converted into molecules by [34] [95]

$$P_{FbM} = 1 - e^{2\pi\delta_{LZ}}, \tag{21}$$

where the Landau-Zener parameter, (δ_{LZ}^{ho}), for a harmonic trap is defined as [104] [171]

$$\delta_{LZ}^{ho} = \frac{\sqrt{6}\hbar}{\pi 2 M a_{ho}^3} \mid \frac{a_{bg}\Delta}{\dot{B}} \mid, \tag{22}$$

where a_{ho} is the harmonic oscillator length of the confining potential, M is the reduced mass, and $\dot{B}$ is the change rate of the magnetic field across the resonance [34].

From these equations above, equation 21 and 22, it can be seen that the efficiency is related to the change rate of the magnetic field, as well as to the width of the resonance. This means that at very slow change rate a complete transition of population should occur, and for all considered coupling mechanisms with narrow resonances it is even more critical to vary the field smoothly enough. Unfortunately, we have to take into account that there will always be some diabatic influences that reduce the efficiency [25].

Magnetic range and resolution

To carry out the magnetoassociation process using FRs, the required range and resolution of the magnetic field must be defined [25]. Based on the Breit-Rabi diagrams the correct B-field is chosen. The required resolution is related to the resonance separation. The resonance separation is the spacing between two Feshbach resonances. It can be derived from the ratio of the hyperfine structure splitting of the excited molecular state, $\Delta E_{hpf,mol}$, and the difference in the magnetic moments of the two states, $\Delta\mu = \mu_{scat} - \mu_{mol}$, times the magnetic field of the FR, B_{FR} [25],

$$\Delta E_{FR} = \frac{\Delta E_{hpf,mol}}{\Delta\mu \cdot B_{FR}}. \tag{23}$$

If the hyperfine splitting is small compared to $\Delta\mu \cdot B_{FR}$ of the FR, the last bound states of the excited potential are involved in the FR. When the hyperfine structure is large compared to $\Delta\mu \cdot B_{FR}$, the deeper bound states of the excited potential can induce the resonance [25]. This magnetic field resonance separation depends on the mass of the particles that are involved. For lighter atoms, this range can be a few ten orders higher in magnitude than for heavier atoms [25].

Detection and Improvement

Characteristic experimental signatures of Feshbach molecules are assigned to a disappearance of the atom number during the magnetic field ramp, as can be seen in figure 9 [9]. To not confuse the dissappearance due to inelastic collisions with FRs, a reverse of the magnetic ramp is used for the indication of the amount of formed Feshbach [25]. In this

reverse of the magnetic ramp the recovery of the atom out of Feshbach molecules is measured and the yield can be calculated [59] in [98], [25].

To improve the yield and reduce the three-body collisions after molecule formation, the molecules have to be protected. The most common protection method is to confine the molecules in a lattice. Another method is to remove atoms by a field gradient ramping or a near-resonant light. Both selectively affect the atoms leaving only the Feshbach molecules [53].

A higher control of the magnetic field would contribute to the efficiency of the molecule formation using magnetoassociation, as can be derived from the Landau-Zener model presented in equation 21. Unfortunately, since there is not much demand for these high magnetic field control, no market exists for this technical equipment with such a power supply. The challenge is allocated to the few research groups exploring this field to generate the enormous accurate control themselves. The Schreck strontium quantum gas group currently achieved to do this and will try it out on atom pairs soon.

Optical Feshbach resonances

A FR can also be induced by optical methods. In these methods a laser field couples the scattering state to a molecular level in an electronically excited molecular potential [88]. Therefore the resonance position of optical FRs corresponds to the laser frequency, and the resonance width is determined by the laser intensity. The crucial difference between magnetic and optical Feshbach resonances is the finite lifetime of the resonance state due to spontaneous emission [25]. The precise details will not be discussed in this report, but a detailed review of optical Feshbach resonances can be found in reference [88].

5.3 Feshbach resonances in RbSr

If we follow the theory of the interaction potential for the ground state RbSr molecule, $^2\Sigma$, given by equation 20, no coupling would arise since V_ℓ has only diagonal terms in ℓ and with $s_{Sr} = 0$ no spin-spin term will arise [25]. However, Zuchowski *et al.* came up with a coupling mechanism in the RbSr molecule caused by a modification of the Rb hyperfine states due to the presence of the Sr atom [177]. This coupling mechanism leads to narrow resonance widths on the orders of a few mG (compared to typical widths of $1 - 300$ G) [177] [34]. This theory was further developed by research into coupling mechanisms of alkali-metals atoms in combination with Yb atoms [21] [22]. The broadest resonance width for the RbSr molecule is now predicted to have a value of a few 10 mG, occuring in some isotopic combinations at very high magnetic fields above 1000 G [10] [27].

Experimentally, FRs in mixtures of $^{87/88}$Sr atoms and ^{87}Rb atoms have been observed by Barbé s*et al.* [9]. The FRs were observed through loss spectroscopy of ^{87}Rb atoms depending on an applied field and the presence of Sr atoms. An overview of the observed loss detections allocated to FRs are shown in figure 9. It can be said that the FRs rely on the magnetic moment of the ^{87}Rb atom, since the Sr atoms has no, or very little, contribution to the magnetic moment. Therefore the resonance positions from the

^{87}Rb Breit-Rabi formula have been used to convert to the zero-field binding energies of the molecular states [124] [9]. The experimentally measured and theoretically calculated widths of the FRs for RbSr molecules are listed in table 1.

Table 1: An overview of the properties of detected FRs in RbSr by the Schreck strontium quantum gas group. The scattering state is denoted by $[f, m_f]$, the Feshbach molecule by its molecular state*, m_f M_L. B(G) presents the magnetic field where the resonance occurs. δ_{exp} is the experimental resonance width measured, and Δ_{calc} is the resonance width calculated according to the Golden Rule Approximation [22]. The FRs are allocated to couplings mechanisms that are expained in the following section. Reproduced from [9].

$[f, m_f]$	(mol. state*, m_f, M_L)	B (G)	δ_{exp} (mG)	Δ_{calc} (mG)	cpl. mech.
		^{87}Sr-^{87}Rb			
$[2, +1]$	(B,+2,0)	474.9(4)	373(7)	0.04	II
$[2, 0]$	(B,+1,0)	435.9(4)	378(7)	0.07	II
$[2, -1]$	(B,0,0)	400.0(4)	247(4)	0.07	II
$[2, -2]$	(B,-1,0)	367(4)	260(5)	0.04	II
$[1, -1]$a	(D,-2,0)	295.4(4)	372(10)	0.33	II
$[1, -1]$b	(C,-2,mix)	420.9(4)	386(11)	0.002	III
$[1, -1]$c	(D,-1,0)	521.5(4)	366(3)	2.4	I, II
$[1, 0]$a	(E,-1,-1)	B_1 = 278.2(4)	30(3)	0.00009	III
	(E,-1,-2)	B_1+ 0.081(2)	58(4)	0.00011	III
$[1, 0]$b	(F,-1,0)	397.3(4)	207(4)	0.02	II
$[1, +1]$a	(E,0,0)	B_2 = 295.0(4)	24(3)	0.00002	III
	(E,0,-1)	B_3+ 0.083(2)	35(3)	0.00009	III
	(E,0,-2)	B_2+ 0.162(2)	30(1)	0.00011	III
$[1, +1]$b	(F,0,0)	432.5(4)	213(6)	0.02	II
		^{88}Sr-^{87}Rb			
$[1, +1]$	(G,+1,0)	365.8(4)	105(2)	0.05	I

*molecular state (n, F, L): B=(-2,2,0), C=(-4,2,2), D=(-4,2,0), E=(-2,1,2), F=(-2,1,0) and G=(-4,2,0), where n = electronic level, F = molecular hyperfine state, and L= total angular momentum

The discrepancies between experimental and theoretical resonance widths (according to the Golden Rule Approximation [22]), δ_{exp} and Δ_{calc} respectively, in table 1 can be explained by collisional and thermal broadening, and magnetic field instabilities [54]. Derivation of the experimentally observed widths is involved and has not been pursued.

Collisional broadening due to collisions between the particles causes extra loss detection. Thermal broadening causes a shift in the hyperfine energy state, leading to a shift of the resonance positions. Additionally, particles follow a Boltzmann distribution for their position, dependent on the temperature (e^{U/k_bT}) [54], which causes additonial width broadening. B-field instabilities have a significant contribution to the measured resonance width, since fluctuations disturb the position where the resonance occurs [113].

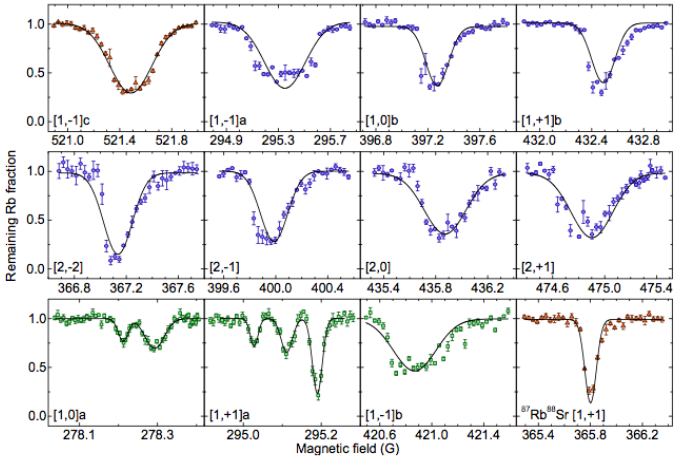


Figure 9: Detected magnetic field dependent loss of Rb atoms by the Schreck Sr Group. The fraction of the remaining Rb atoms are normalized to unity. The panels are labeled by the Rb atomic state $[f, m_f]$. In case of more resonances occuring with the same atomic state, indices are added to distinguish. The colors and symbols represent the mechanism that is allocated to the resonance,expained in the following section. The orange triangles represent mechanism I, the orange triangles mechanism II and the green squares mechanism III. The lower-right panel assigned to FR of ^{88}Sr-^{87}Rb, the other panels are allocated to the FRs of the ^{87}Sr-^{87}Rb molecule. The figure is copied from [9].

Coupling Mechanisms for RbSr

Now that we have seen FRs do exist for the RbSr molecule we can discuss the theoretical coupling mechanisms behind them. Several coupling mechanisms can be invoked by explaining the formation of RbSr Feshbach molecules [177] [21] [22]. To find the elements that cause the coupling, e.g. to find off-diagonal elements in the solutions of the SE (equation 4), we consider the effective Hamiltonian of an atom pair as well as the effective Hamiltonian for a $^2\Sigma$ diatomic molecule [177].

The collision Hamiltonian of an atom pair is expressed as [21]

$$\hat{H}_{eff,collision} = \frac{\hbar^2}{2\mu}\left(\frac{-1}{r}\frac{d^2}{dr^2}r + \frac{\hat{L}^2}{r^2}\right) + \hat{H}_\alpha + \hat{H}_\beta + \hat{V}(r). \tag{24}$$

In this Hamiltonian, the first part represents the kinetic energy where μ is the reduced mass and $\hat{L}$ is the angular momentum operator. $\hat{V}(r)$ represents the interaction potential [177] as is given in equation 19. $\hat{H}_\alpha$ and $\hat{H}_\beta$ [1],

$$\begin{aligned} \hat{H}_\alpha &= \zeta_\alpha \hat{i}_\alpha \cdot \hat{s}_\alpha + (g_\alpha^e \mu_B \hat{s}_{\alpha z} + g_\alpha^{nuc} \mu_N \hat{i}_{\alpha z})B \\ \hat{H}_\beta &= g_\beta^{nuc} \mu_N \hat{i}_{\beta z} B, \end{aligned} \tag{25}$$

represent the Hamiltonians for an alkali-metal atom α and a closed shell atom β respectively based on their nuclear and electronic spin [177]. ζ is the hyperfine coupling constant that determines the magnitude of the nuclear i and electronic s spin coupling. ζ is dependent on the distance to the nucleus and summarizes the physics of the coupling depending

on the values of i and s. $\hat{i}$ and $\hat{s}$ are the nuclear and electronic spin operator respectively. $g_{\alpha/\beta}$ are the g-factors, and μ_B and μ_N are the Bohr and nuclear magneton respectively [21].

When we consider the eigenstates of this interaction Hamiltionian, we have at zero B field the $|F, M_f\rangle$ states as eigenstates. However, at finite B field, the eigenstates, that are still labeled by $|F, M_f\rangle$, are mixed states with respect to the zero field $|F, M_f\rangle$ eigenstates. These mixed states are not solutions of the effective Hamiltonian anymore. This means that these states are no longer diagonal. During the collision, the non-diagonal terms are varied leading to the coupling required for the FRs process [177].

Mechanism I: Coupling from the modification of the Rb hyperfine coupling by the presence of another atom

The first explanation for a coupling mechanism is found by a theoretical prediction of Zuchowski *et al.* [177] [22]. This prediction states that the coupling relies on a perturbation of the electron distribution of the Rb atom due to the presence of the Sr atom. Something that previously has been neglected in the collision Hamiltonian, recalling $V(r)$ in equation 19 and 20.

The presence of another atom can cause a modification in the hyperfine coupling constant that results in

$$\zeta(r) = \zeta + \Delta\zeta(r), \tag{26}$$

where $\Delta\zeta$ is the change due to a modification of $\langle\hat{i}\cdot\hat{s}\rangle$. This $\Delta\zeta$ causes a perturbation to the wave function breaking the symmetry of the wave function. The caused $\langle\Delta\zeta\hat{i}\cdot\hat{s}\rangle$ is not part of the effective Hamiltonian of the free atom, but is part of the interaction potential and thus produces off-diagonal elements [177]. Hence we can express the total interaction operator by [21]

$$\hat{V}(r) = V(r) + \Delta\zeta_\alpha\hat{i}_\alpha\cdot\hat{s} + \Delta\zeta_\beta\hat{i}_\beta\cdot\hat{s} \tag{27}$$

where $V(r)$ is given in equation 20 and $\Delta\zeta_{\alpha/\beta}$ arises from the perturbation. The presence of the Sr atom perturbs the electron distribution of the Rb atom which causes the perturbation $\langle\Delta\zeta_\alpha\hat{i}_\alpha\cdot\hat{s}_\alpha\rangle$ [177]. By obeying the selection rules, only states of equal m_f are coupled in this mechanism. Therefore the coupling only depends on atomic state with $f = 1$, and molecular states with $f = 2$ as shown in table 1.

Mechanism II: Coupling due to polarization of the nuclear spin density by a valence electron

The second mechanism, proposed by Hutson and Brue, is found to exist due to a change of the hyperfine coupling of the nuclear spin of the ^{87}Sr atom [21]. The presence of valence electrons of the Rb atoms perturbs the nuclear spin of ^{87}Sr atom. When the Rb atom approaches the Sr atom, a polarization of the spin density of the Sr atom occurs. This polarization of the spin density creates a change in the hyperfine coupling between the molecular spin of the molecule and the nuclear magnetic moment of the Sr atom which causes the perturbation $\langle\Delta\zeta\hat{i}_{sr}\cdot\hat{s}_{mol}\rangle$, which is like mechanism I not part of the effective Hamiltonian [21]. This coupling of the molecular valence electrons with the nucleus of

Sr causes an exchange in their angular momentum. The change is rather large relative to the change in the hyperfine coupling of the Rb atom. By conserving M, the coupling obeys the selection rule $\Delta m_f^{atom-mol} = \pm 1$ while being able to occur at the same f [9]. The hyperfine coupling constant of the Sr atom is also modified by the presence of the Rb atom with some additional small contributions that are coming with it as is the case in coupling mechanism I given above. But this latter effect is much smaller for the Sr atom than the emerging hyperfine coupling of the molecular spin [21].

Mechanism III: Coupling through anisotropic interaction of the electron spin

The third mechanism that is found for the RbSr molecule is rather complicated and the production efficiency of Feshbach molecules is very small as can be seen in table 1 [9]. The coupling mechanism relies on anisotropic effects of the coupling that are not taken into account in the first two mechanisms. The first two mechanisms are described by contact interactions, which only are based on the parameter r, i, and s. In these parameters there is no knowledge about any angle that the coupling includes.

To find the anisotropic effect, we approach the system from a molecular perspective by considering the effective Hamiltonian for a $^2\Sigma$ diatomic molecule, consisting of a sum of a rotational-fine structure, hyperfine structure, Stark, and Zeeman Hamiltonian [1],

$$\hat{H}_{eff} = \hat{H}_{rfs} + \hat{H}_{hfs} + \hat{H}_s + \hat{H}_z, \tag{28}$$

with $\hat{H}_{hfs}$ being [1]

$$\hat{H}_{hfs} = \sum_{i=1}^{2} e\hat{Q}_i \cdot \hat{q}_i + \sum_{i=1}^{2} \hat{S} \cdot \hat{A}_i \cdot \hat{I}_i. \tag{29}$$

The $\hat{H}_{hfs}$ includes the terms representing the interaction between the electronic S and the nuclear I spin of the molecule, as well as the interaction between the quadrupole tensor $(\hat{Q}_i)$ and the electric field gradient tensor, $(\hat{q}_i)$ of nucleus i [1]. Therefore the coupling constants in equation 29 are eQq and A. A has an isotropic and an anisotropic component. In the anisotropic part, the quantum number L is not conserved and no rotational symmetry exists, concerning the nuclear rotation that is included in the model [1]. A spin-rotation interaction occurs between L, the valence electron, and nuclear spin of the Rb atom. Here an atomic s-wave couples with molecules with rotational quantum number $L = 2$ [177]. Furthermore an interaction between the nuclear quadrupole moment eQq and the electron density of the Sr atom is caused by the distortion of the electron density due to Sr [177]. This quadrupole moment can also couple $\Delta L \neq 0$. When the coupling only involves an interaction due to the angular momenta of the Rb atom, $\Delta m_f = -\Delta m_\ell$ is obeyed. Including the fermionic Sr atom in the coupling, a selection rule of $\Delta m_f = \pm 1$ is followed [9].

6 Stimulated Raman Adiabatic Passage

This chapter will discuss, after a brief historical overview of STIRAP, the fundamental physics of coherent excitations by laser pulses, followed by an explanation of the STIRAP process. The chapter will be closed with the discussion of the latest developments of a STIRAP scheme for the RbSr molecule.

STIRAP allows efficient and selective population transfer between two states with the help of an energy shifted intermediate state as is shown in figure 10 [161]. By adiabatic evolution, the total interacting system creates an eigenstate where the intermediate state only serves as a coupling between the initial and target state but is never populated as shown in equation 35. This eigenstate does not include the intermediate state and is the key feature of its high efficiency since in this way spontaneous decay is avoided. STIRAP is also robust against small variations of experimental conditions, which makes it a promising method [162].

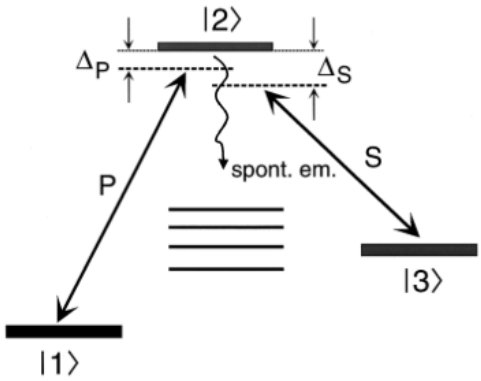


Figure 10: A three level excitation scheme. The initial state, $|1\rangle$, lies in this scheme lower than the final state, $|3\rangle$. The pump laser P couples $|1\rangle$ with the intermediate state, $|2\rangle$, from which spontaneous emission can occur. The dump laser S couples $|3\rangle$ with $|2\rangle$. $\Delta_{P/S}$ denote the detuning from the transition frequency between the state and the applied laser frequency. When the total detuning is zero and the pulse sequency has the correct timing, $|2\rangle$ can be avoided to be populated as is explained in the text. Figure is copied from [11].

STIRAP showed to be promising in inducing coherent two-color photoassociation and to serve as the last step in the pathway to obtain ultracold molecules in the ground state [85] [38] [105]. In 2005, the first atom-molecule dark states in a BEC and a DFG were reported by Winkler *et al.* [165]. Two years later they reported the first STIRAP transfer of Feshbach molecules into chemically stable bound molecules [164]. Detailed theoretical research have been carried out in proposed STIRAP schemes for various AK-AKE molecules [130]. Experimental studies of STIRAP in these AK-AKE molecules have only been carried out for LiCa [142], RbCa [129] and RbSr [124] [6] [103] [99] [27].

6.1 Theory STIRAP

Coherent excitation in a three level-system

The STIRAP process makes use of three energy levels; an initially populated state ($|1\rangle$), an intermediate state ($|2\rangle$), and a target state ($|3\rangle$) [161]. The intermediate state couples with the initially populated state and as well as with the target state. The coupling is induced by coherent radiation using laser pulses [161]. The dynamics of excitation in a three level system due to coherent interaction with an applied laser field can be described by a time-dependent SE [138] [162],

$$i\hbar\frac{t}{dt}\Psi(t) = \hat{H}(t)\Psi(t), \tag{30}$$

where the state vector $\Psi(t)$ presents a three-component column vector consisting of the three states with corresponding probability amplitudes C_n,

$$\Psi(t) = [C_1(t), C_2(t), C_3(t)]^T, \tag{31}$$

where n represents the state. The Hamiltonian includes the eigenenergies of the states as well as the interactions of the light with the atoms [100]

$$\hat{H}(t) = \hbar \begin{pmatrix} 0 & \Omega_P(t) & 0 \\ \Omega_P(t) & \Delta_P & \Omega_S(t) \\ 0 & \Omega_S(t) & \Delta_P - \Delta_S \end{pmatrix}, \tag{32}$$

where the diagonal terms are the energies that corresponds with the energies of the bare states lifted by their interaction with the laser field. Here we neglect the fast frequency terms of the light matter interaction by using the Rotating Wave Approximation (RWA)[65]. The energy of the $|1\rangle$ is set to zero and used as a reference. Δ_P and Δ_S are determined by the energy states and the frequency of the laser light [11],

$$\begin{aligned} \hbar\Delta_P &= E_1 - E_2 - \hbar\omega_P \\ \hbar\Delta_S &= E_2 - E_3 - \hbar\omega_S, \end{aligned} \tag{33}$$

where E_n is the energy of the individual states and ω_P and ω_S are the carrier frequencies of the applied lasers denoted by P and S.

The off-diagonal terms arise from the laser-atom interaction and are represented by $\Omega_{P/S}$. These Ω_P and Ω_S are called the Rabi frequencies and represent the frequency of population oscillation. Those frequencies are associated with the strength of the interaction due to a periodic exchange of energy between light and matter [65]. Their values are determined by the corresponding transition dipole moment between the states and the respective laser intensity that is sinusoidally oscillating, which we can derive from the electric field amplitude [161] [65],

$$\Omega_{P/S} = \frac{d_{12/23} \cdot \epsilon_{P/S}}{\hbar}, \tag{34}$$

where $d_{12/23}$ is the atomic transition dipole moment and $\epsilon_{P/S}$ is the laser electric field amplitude. For the coupling of the $|1\rangle$ and the $|2\rangle$ a pump laser is applied, which we denote by P.

For the coupling of the $|3\rangle$ with the $|2\rangle$ a dump laser is applied, which we denote by S [161]. To obtain coherence between the states, a two-photon detuning is required to be zero. Since the three states in a STIRAP process have a Λ linkage pattern we can derive that $\delta = \Delta_P - \Delta_S$ and thus $\Delta_P = \Delta_S$ must be obeyed [162].

Adiabatic states

The existence of the adiabatic state Φ_0 is the key feature of the STIRAP process. This state can be found by the instantaneous eigenstates of the time-dependent SE with $\hat{H}$ given in equation 32 [138] [162],

$$\begin{aligned}
\Phi_+(t) &= \psi_1 \sin\phi(t) + \psi_2 \cos\phi(t) + \psi_3 \cos\theta(t) \sin\phi(t) \\
\Phi_0(t) &= \psi_1 \cos\theta(t) - \psi_3 \sin\theta(t) \\
\Phi_-(t) &= \psi_1 \sin\theta(t) \cos\phi(t) - \psi_2 \sin\phi(t) + \psi_3 \cos\theta(t) \cos\phi(t),
\end{aligned} \tag{35}$$

where ψ_n presents the non-interacting bare state. $\theta(t)$ and $\phi(t)$ are the mixing angles that are defined by $\theta(t) = \tan^{-1}[\Omega_P(t)/\Omega_S(t)]$, $\phi(t) = \tan^{-1}[\sqrt{\Omega_P^2(t) + \Omega_S^2(t)}/\Delta]$, and ψ_i is the unperturbed bare state.

The Φ_0 state is described by the two bare states 1 and 3, see equation 35. The corresponding amplitudes of this state are dependent on the mixing angle that is determined by the ratio of intensities of the laser pulses [64]. An adiabatic evolution maintains alignment of this Φ_0 state. When we combine this feature with the correct timing of the laser intensities, the system can transfer population from state 1 to state 3 without populating state 2 [161]. This given, the timing of the two laser beams is the key parameter to achieve efficient transfer between state 1 and 3 [162].

The eigenvalue of Φ_0 is $\varepsilon_0(t) = 0$ and the eigenvalues of $\Phi_{+/-}$ are $\varepsilon_{+/-}(t) = \Delta \pm \sqrt{\Delta^2 + \Omega_P^2(t) + \Omega_S^2(t)}$ [161]. The eigenvalues $\epsilon_{+/-}$ when $\Omega_P \neq \Omega_S$, can be explained by the Autler Townes splitting. This is a dynamic Stark splitting that occurs due to coupling with the applied electric field. The coupling causes a splitting of the molecule energy state. Its derivative can be found in reference [29].

6.2 Experimental procedure of STIRAP

To allow an efficient population transfer without loss due to incoherence, several conditions have to be fulfilled. Among others these are the frequency, intensity, timing and change rate of the applied laser [161] [162].

Adiabatic evolution

The system will be aligned to the Φ_0 state as long as the evolution is adiabatic. This is when the variation in the mixing angle θ is slow enough to let the state vector adjust to the evolution. The adiabatic evolution has to be obeyed in local adiabatic conditions as well as in global adiabatic conditions. At the local level, this means that the splitting between the eigenvalues of the states must be much larger than the coupling between

them [18] [90],

$$\begin{aligned} &\mid \varepsilon_0 - \varepsilon_{+/-} \mid \gg \mid \langle \dot{\Phi}_0 \mid \Phi_{+/-} \rangle \mid \\ &\mid \varepsilon_0 - \varepsilon_{+/-} \mid \gg \mid \frac{\dot{\Omega}_P \Omega_S - \Omega_P \dot{\Omega}_S}{\Omega_P^2 + \Omega_S^2} \mid . \end{aligned} \tag{36}$$

The global adiabatic conditions can be found in the requirements of the pulse area. This can be derived from the $\dot{\theta}$, since $\dot{\theta}$ is proportional to the inverse of the pulse width, determined by timepulse t. By considering the restriction of the resonance excitation ($\delta = 0$) we can find that [161]

$$\sqrt{\Omega_P^2 + \Omega_S^2} \gg \mid \dot{\theta} \mid \propto t^{-1}. \tag{37}$$

Hence $\Omega_0 \cdot t \gg 1$, where $\Omega_0 = \sqrt{\Omega_P^2 + \Omega_S^2}$ we can see the requirement of a large pulse area [169] as seen in equation **??**.

Pulse delay

The pulse delay τ between the two laser pulses has a significant influence on the efficiency of the population transfer. First of all this occurs because of the adiabatic conditions. Secondly by completeness of the projection of the state vector $\Psi(t)$ onto the Φ_0 state at the initial and final time [162].

A small τ causes a large overlap of the laser. In this way θ is almost constant during the process and hence the $\dot{\theta}$ is almost zero. This results in a good adiabaticity. However, a problem is found at the early and final times. In these moments θ changes too fast from 0 to θ_0 and too fast from θ_0 to $\pi/2$ due to the small value of τ. This fast change results into non-adiabatic couplings and therefore loss of coherence [162].

At the other extreme, having a large τ between pulses ensures a complete projection of $\Psi(t)$ onto the Φ_0 state at early and at very late times, and $\dot{\theta}$ is rather constant. However the large τ comes along with a small spatial overlap of the lasers. During this very small spatial overlap θ rises very fast from 0 to $\pi/2$, resulting in a large non-adiabatic coupling [162]. To determine the optimum τ we have to include the pulse shape. For a Gaussian pulse the τ has to be slightly larger than the pulse width so that the mixing angle changes slowly and smoothly in time [160]. It can also be derived from equation 36 that the Autler-Townes splitting scales proportionally to $\dot{\theta}$.

Laser pulse sequence

The lasers used in the STIRAP process are on or near resonance and partially overlapping in time [64]. A counterintuitive pulse ordering is needed to couple the two state in the correct order. Initially, a laser field ratio where $\Omega_S \gg \Omega_P$ and θ being zero is required. In this way Φ_0 coincides with only state 1 but allows coupling between state 3 and 2 as shown in panel (a) in figure 11, where $Laser2$ and $Laser1$ correspond with the dump laser S and pump laser P respectively, and state $|b\rangle$, $|e\rangle$, and $|a\rangle$ correspond with state 3, 2, and 1 respectively. Finally, a laser field ratio where $\Omega_P \gg \Omega_S$ and θ being $\pi/2$ is required. Then Φ_0 coincides with state 3 no population transfer back to state 1 is possible as shown in figure panel (e) in figure 11 [162].

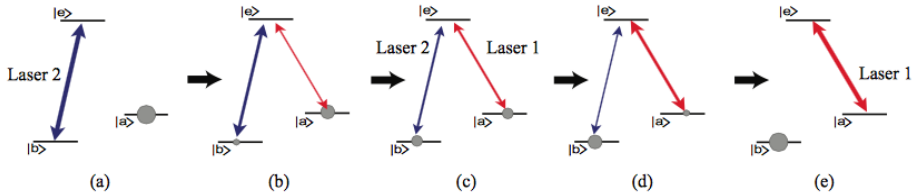


Figure 11: The STIRAP laser pulse sequence in five stages to allow adiabatic transfer from state 1 to state 3 thats keeps alignment to the darkstate. Panels (a)-(e) represent the laser intensities with corresponding population over time in the STIRAP process, where (a) represent the initial state with $\Omega_2 \gg \Omega_1$ and only state $|a\rangle$ is populated. Panel (e) shows the final stage with $\Omega_1 \gg \Omega_2$ and only state $|b\rangle$ is populated. The stages a-e correspond with stage 1-5 in figure 12 and in the text. *Laser*2 and *Laser*1 correspond with the dump laser S and pump laser P respectively, and state $|b\rangle$, $|e\rangle$, and $|a\rangle$ correspond with state 3, 2, and 1 respectively in figure 12 and in the text. See text for details. Figure is copied from [59] in [98].

By following the conditions given in the theory above, the experimental process for STIRAP is clearly explained in five stages by Vitanov, Rangeloc, Shore and Bergmann as shown in figure 12 [162].

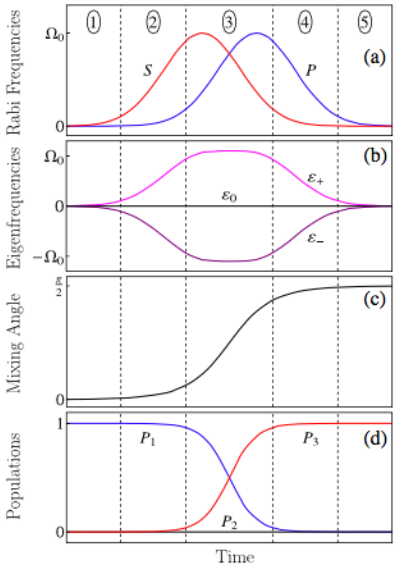


Figure 12: A STIRAP process induced by Gaussian pulses of equal peak values and a total detuning of zero. The process is divided in five stages, where per stage the Rabi Frequency, the eigenfrequencies, the mixing angle and the population according to time is shown. See text for details. Figure is copied from [162].

In **stage 1**, first a S-pulse of a dump laser will be turned on to couple the unpopulated states 3 and 2 with each other. The coupling causes the Autler-Townes splitting that leads to a separation between the eigenvalues of the two adiabatic states Φ_+ and Φ_-. The P-pulse intensity in this stage is zero, therefore the mixing angle θ is zero and Φ_0 coincides with state 1 as can be derived from equation 35.

In **stage 2**, the S-pulse is ramped on towards strong intensity which allows for the P-pulse to be turned on. The stronger intensity increases the Autler-Townes splitting. A strong coupling exist between state 3 and 2. The state vector Φ_0 deviates a bit from the state 1 as can be deduced from the mixing angle, however no transition will occur between state 1 and state 2 due to destructive interference between the Autler-Townes components.

In **stage 3**, the S-pulse is ramped off and the P-pulse is ramped on. At the point where both lasers are equal in intensity, Φ_0 is described by equal amplitudes of state 1 and

state 3. At this point the slope of the mixing angle and the Autler-Townes splitting are at their maxima. From this point the lasers show an exchange in character; the Autler-Townes splitting starts to reverse; the mixing angle starts to deflect towards $\pi/2$; and the population starts to inverse.

In **stage 4**, the functions of lasers S and P are opposite in this state compared to stage 2. The intensity of the S-pulse is almost zero, while the P-pulse is ramped off. The state vector Φ_0 becomes more aligned with a minus state 3 character. The almost zero-intensity of the S-pulse impedes to induce transitions from state 3 to state 2. Simultaneously the P-pulse strongly couples the state 1 and 2. Due to the Autler Townes splitting, similar as in stage 2, the population in state 3 is now protected.

In **stage 5**, the process is opposite to the first stage. No S-laser is present anymore and the P laser is slowly ramped off, bringing the Autler Townes splitting to zero. The mixing angle being $\pi/2$ results in Φ_0 coinciding with minus state 3.

Other factors of influence

Although the largest contribution in the efficiency of the STIRAP process is from the time sequence and the optimum delay of the laser pulses, several other aspects have to be mentioned [162]. The phase fluctuations between the two fields, degeneracy of energy levels, and the dependence of the velocity of the atoms on the detuning Δ (which can cause a Doppler shift) also must be taken into account as they can affect the efficiency of the transition. Their contributions are discussed in detail in reference [162].

Detection and Improvement

The production of transferred molecules are demonstrated by a STIRAP cycle. A STIRAP cycle is a forward and backward process of STIRAP, where the backward process is carried out with a time mirrored pulse sequence [144]. In between the two processes the remaining population in the initial state is removed.

The efficiency of the method is measured by detecting the population of particles in the initial state after the backward STIRAP with the help of absorption images. Improvements in the efficiency of STIRAP were shown by Ciamei *et al.*, and were demonstrated in the formation of Sr_2 molecules out of ultracold Sr atoms [26]. In this experiment compensation beams were used to minimize shifts in the energy states caused by interaction with the optical lattices leading to a significant improvement of the yield.

6.3 STIRAP scheme for RbSr

A STIRAP scheme is proposed for the production of the ground state RbSr molecule, because direct transfer of the weakly-bound RbSr Feshbach molecule to the ground state is not possible due to lack of a significant value in wavefunction overlap [130].

An efficient STIRAP scheme requires the knowledge of properties of the three states involved in the process [130]. The starting point for refinement of efficient schemes are theoretical investigations of the PECs, which are then followed by a more detailed analysis of the vibrational states that are most suitable. The required wavelengths for proper

population transfer can be determined by the differences in eigenenergies of the involved states [178].

Theoretical investigations

The electronic structure of the RbSr molecule in its ground and lowest excited state have been profoundly examined by several groups using ab initio methods [72] [177] [67] [128] [24] [130]. In the beginning, theoretical calculation of the RbSr molecules only contained the ground state PEC of a RbSr molecule [72] [177] [67]. This was extended by several groups to the investigation of the lowest excited asymptotes of RbSr molecules [178] [128] [24] [130]. By further research into the transition probabilities, with that analyzing vibrational levels, proposed STIRAP schemes can be found by Chen *et al.* and Pototschnig *et al.* nowadays [24] [130].

Although the description of computational methods is beyond the scope of this report, we can discuss the general pathway very briefly. A detailed explanation can be found in several computational books [35]. In general theoretical calculations first starts with ab initio calculations to find characteristics of PECs. By assuming the Born-Oppenheimer approximation, the PECs can be diagonalized and optimized to find transition probabilities. Finally, based on the transition probabilities, intermediate states are chosen to set up an optimum STIRAP scheme and to calculate its predicted efficiency [35] [128] [67] [24] [130]. This pathway is roughly the same for all theoretical investigations, and the values at long-range do in general agree for different methods. However, significant discrepancies easily appear from small differences in methods at short range where the chemical potential has a large contribution. Because of this, results of theoretical studies have to be read with care: when analyzing and comparing the theoretical calculations it has to be taken into account which parameters are assumed, which particular method is used including the level of accuracy and interactions, and what is actually optimized. The differences in outcomes due to the choice of method can be clearly seen in the differences in found value for the potential depth of the RbSr molecule ground state, listed in table 2. Moreover, it has to be mentioned that the theoretical calculations are purely based on optical decay and merely serve as a starting point in experiments since any experimental influences, among others the δ-shift due to the trapping light that might cause decay, are excluded [26] [39].

Experimental spectroscopic research

In order to create molecules at ultracold temperatures the precision of ab initio calculations are not enough to rely experiments on. Experimental spectroscopic research is needed to complement theoretical calculations [27]. Experimental spectroscopic research of RbSr is done by the group of Ernst and by the group of Schreck [103] [99] [27].

Ernst his group carried out a spectroscopic study of the ground state transition energies of the RbSr using helium droplet as a surface to relax RbSr into ro-vibrational ground state [103] [99].

The group of Schreck performed three types of spectropy experiments to investigate the ground and second excited electronic states of the RbSr molecule. Photoassocation spectroscopy of ultracold atoms have been provided data of weakly-bound levels and from

Table 2: An overview of calculations for the ground state well depth, D (cm^{-1}), and equilibrium distance, R_e (Å), by different research groups using different computational methods.

Source	Method	Ground state Depth D (cm^{-1})	eq. distance R_e (Å)
Zuchowski [177]	RCCSD(T)	1000	4.69
Guerout [72]	FCI + ECP + CPP	1073	4.60
Gopakumar [67]	CCSD	916	4.72
Chen [24]	KR + MRCI	1018	4.67
Zuchowski [178]	RCCSD(T)	1041	4.67
Pototschnig [128]	MCSCF + MRCI	2074	4.59
Ernst [130]	CCSD	778	4.79
	MRCI	1298	4.56
	CASPT2	1198	4.58
Ciamei [27]	joint fit of experimental data with [178] and [130]	1152	-

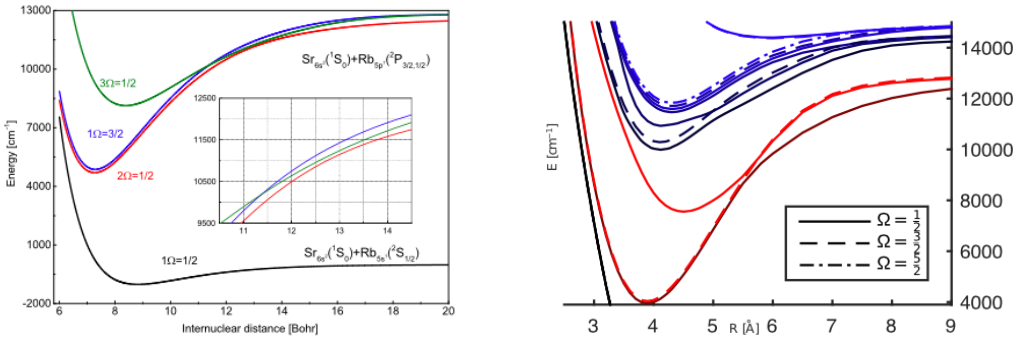
that long-range behaviour of the PECs [88] [27]. Thermoluminescence and laser induced fluorescence (LIF) spectropscopy of hot molecules allowed to determine the deeply-bound levels, the behaviour of the PECs in a range of internuclear distances that is centred around the potential equilibrium distance [150] [27]. Combining the three method led to a model representing the complete spectrum of the $X(1)^2\Sigma^+$ ground state of RbSr [27]. Furthermore the group combined the obtained experimental data with previous calculated ab initio data. This led to new insights of the bottom of the PECs of the ground and second excited electronic state and a new description of the PEC RbSr ground state molecule that accurately represents the their experimental data [27].

Potential energy surface

The lowest excited asymptotes of the RbSr molecule are found as the molecular states $^2\Sigma$ and $^2\Pi$. An excitation in Rb, e.g. Rb(5p ^{2}P) + Sr($5s^2$ ^{1}S), leads to molecular states $^2\Sigma$ and $^2\Pi$. An excitation in Sr, e.g. Rb(5s ^{2}P) + Sr(5s5p ^{3}P) leads to the molecular states $^2\Sigma$ and $^2\Pi$ as well as to states $^4\Sigma$ and $^4\Pi$. In all calculations, the excited energy levels due to an excitation in Sr are found to be higher in energy. These higher lying energy potentials are distinguished by a higher excitation number as shown in figure 13 [24] [130]. When SO-coupling is included, the lowest asymptotes are denoted with values of $\Omega = \mid \Lambda + S \mid$, see table 3. The first values of 2Ω or $3\Omega = 1/2$, and $1\Omega = 3/2$ can be assigned to excitations in Rb. Sr excited potentials have higher values. The $1\Omega = 5/2$ arises from the $^4\Pi$ [130]. A detailed explanation for the spin-orbital term configurations and its assignment in the RbSr molecule can be found in reference [178].

Table 3: An overview of excited molecular states for RbSr, including SO-coupling with their molecular term symbol, corresponding diatomic asymptote and their calculated well depth, $D_e(cm^{-1})$, by [24] and [130]

Ω	$^{2S+1}\Lambda_{\lvert\Lambda+\Sigma\rvert}$	diatomic asymptote	$D_e(cm^{-1})$ [24]	$D_e(cm^{-1})$ [128]
1 (1/2)	$X^2\Sigma_{1/2}$	-	1017.6	1274.2
2 (1/2)	$1^2\Pi_{1/2} + 2^2\Sigma_{1/2}$	Rb $(5p^2P_{1/2})$	7883.1	8569.0
1 (3/2)	$1^2\Pi_{3/2}$	Rb$(5p^2P_{3/2})$	7957.3	8727.6
3 (1/2)	$2^2\Sigma_{1/2} + 1^2\Pi_{1/2}$	Rb$(5p^2P_{3/2})$	4683.6	5252.3

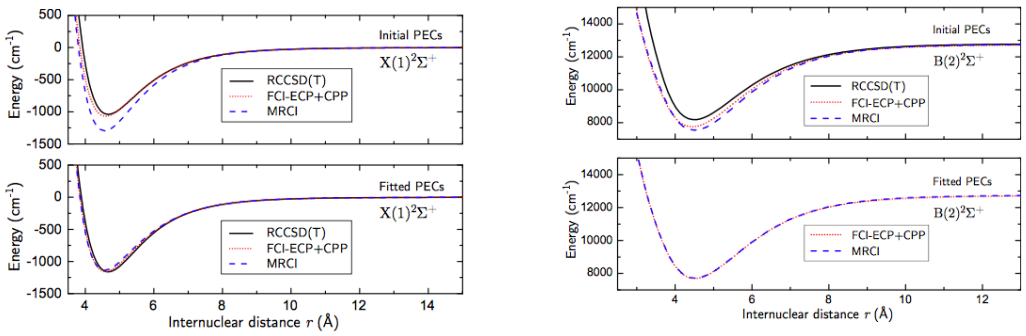


(a) (b)

Figure 13: PECs of excited state of RbSr including SO-coupling. (a) Theoretical calculations of Chen *et al.*. Figure is copied from [24]. (b) Theoretical calculations of Potoschnig *et al.* Figure is copied from [130].

In all theoretical investigations a shallow PEC for the ground state was found, which is a universal character of alkali-alkaline earth dimers [17] [72] [22] [173]. Furthermore, the excited doublet states were found to bind more strongly as shown in figure 13. The inclusion of SO-coupling was found to be necessary for asymptotes with a value of Λ higher than zero to obtain realistic calculations, and has been supported by comparision of experimental values [99].

Ciamei *et al.* used their experimental data of hot and ultracold RbSr molecules in a joint potential fit of the ground state and second excited state. In this fit parameters of ab initio calculations by Zuchowski *et al.* and Pototschnig *et al.* were used to complement missing parameters [178] [130]. The fits with different starting potentials converged towards a unique solution as shown in figure 14. This unique solution is in good agreement with experimental data and constrains a depth of the potential well to $D_e = 1152$ cm^{-1} for the RbSr ground state.



(a) (b)

Figure 14: PECs of the ground state (a) and second excited state (b) of the RbSr molecu. Top panels show ab initio calculations of Zuchowski *et al.* and Pototschnig *et al.*. Bottom panels show PECs fitted to experimental data of Ciamei *et al.* with initial fit parameters determined by Zuchowski *et al.* and Pototschnig *et al.*. Figure is copied from [27].

Transition Dipole Moments

Transition dipole moments (TDM) with respect to their dependence on the internuclear distance have been derived from the PECs. A general trend was found for $\Sigma \leftarrow \Sigma$ excitations to have higher TDM values compared to $\Pi \leftarrow \Sigma$ excitations. At large nuclear distance, which here means > 6 Å, a significant value of the TDM was only found for $X^2\Sigma \leftarrow 2^2\Sigma$ and $X^2\Sigma \leftarrow 1^2\Pi$. Inclusion of SO-coupling revealed significant values of TDM for transitions of $X(\Omega = 1/2) \leftarrow 2(\Omega = 1/2)$, $X(\Omega = 1/2) \leftarrow 3(\Omega = 1/2)$ and $X(\Omega = 1/2) \leftarrow 1(\Omega = 3/2)$. As a result of SO-coupling, additional avoided crossings lead to significant changes in the TDM [130]. The avoided crossings lead to an exchange of angular momentum projection and a change of the shape of the PEC having its consequences for the numerical evaluation of the vibrational levels as shown in figure 13.

Vibrational transitions

Transitions in a STIRAP process occur at the vibrational level. The strongest contributions to low vibrational levels stem from the equilibrium distances between the nuclei, curvature differences and anharmonicity effects. Higher vibrational levels are more affected by long-range behavior. The vibrational transitions are determined by the Franck Condon Factors (FCFs) [24]. These FCFs are derived from the Franck Condon Principle (FCP) [63] [31]. The FCP is based on the Condon approximation, which states that the nuclear motion is stationary with a fixed value compared to the electronic motion considering the time scale of a dipole transition. With this assumption, the total transition probability of a population transfer can be separated into a nuclear and an electronic component,

$$P_{transition} = \left([\text{nuclear overlap}] \cdot [\text{TDM}]\right)^2 . \tag{38}$$

From this it can be seen that although the nuclear component is not affected by the dipole moment transition, a vibronic transition is still proportional to the nuclear overlap of the vibrational wavefunctions of the two states involved in the transition. This nuclear term

is denoted by the FCF [63] [31] [7],

$$FCF_{v''\leftarrow v} = \mid \langle g, v'', J'' | e, v', J' \rangle \mid^2, \tag{39}$$

where g and e are the electronic ground and excited-state respectively, v represents the vibrational state and J is the rotational energy state.

The FCFs can be calculated by ab initio calculations with wavefunctions expanded in electronic, vibrational and rotational levels. Because small FCFs have a low population transfer probability, a much larger laser intensity is required to induce a transition [24]. The FCFs of vibrational levels are used to explore an efficient transition between the three states. A color map of vibrational state overlap for a given electronic transition with a chosen ΔJ is often used as an overview of the FCFs [130]. In this color map FCFs are plotted as a function of the ground state vibrational number v'', and the vibrational number v' in the excited state as shown in figure 15.

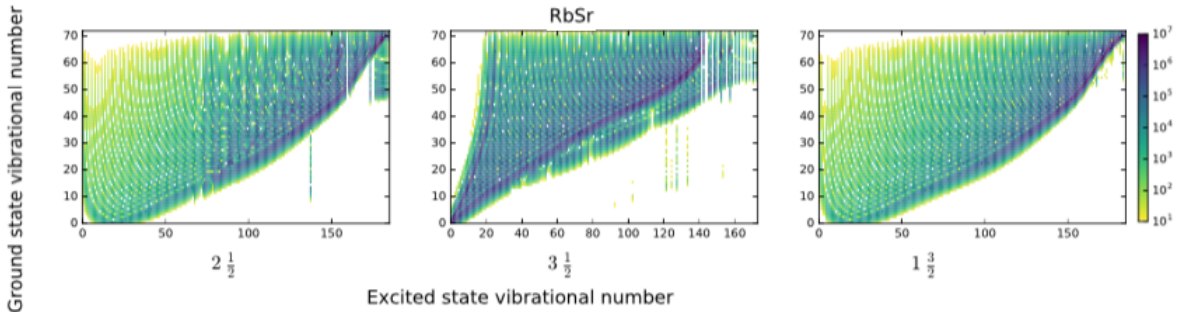


Figure 15: A colormap of vibrational overlap in RbSr for SO-state 2 ($\Omega = 1/2$), 3 ($\Omega = 1/2$), and 1 ($\Omega = 3/2$) (see table 3 for corresponding atomic excitations) calculated with ab initio methods. The SO-coupling is included as distance-dependent spin-orbit matrix elements. Figure is copied from [130].

In these plots, the x-axis represents the excited state that supports the intermediate state. The y-axis represents the vibrational levels in the ground state. A spread out of two branches is found in turning points on the x-axis. A turning point is the position in a vibrational wavefunction where the impulse moment is zero. At the turning points a large nuclear overlap is found for the excited vibrational state with both high and low vibrational states of the electronic ground state. This feature allows pathways to be efficient in a coherent de-excitation and excitation, the feature we search for in an intermediate state. Another method to find the most appropriate intermediate level is to multiply the FCF of the two transitions, F(state 1, state 3) = $\mathrm{FCF}_{1\to2} \times \mathrm{FCF}_{2\to3}$ as shown in figure 16.

Turning points in calculations where SO-coupling was neglected are found in excited doublet states with a vibrational level of approximately $v' = 10$ by Pototschnig *et al.* [130]. In calculations that include SO-coupling, turning points in the $2(\Omega = 1/2)$ state were found in vibrational levels $v' = 18$, $v' = 21$ and $v' = 23$ by [24] as well as by [130] as shown in figure 15 and figure 16.

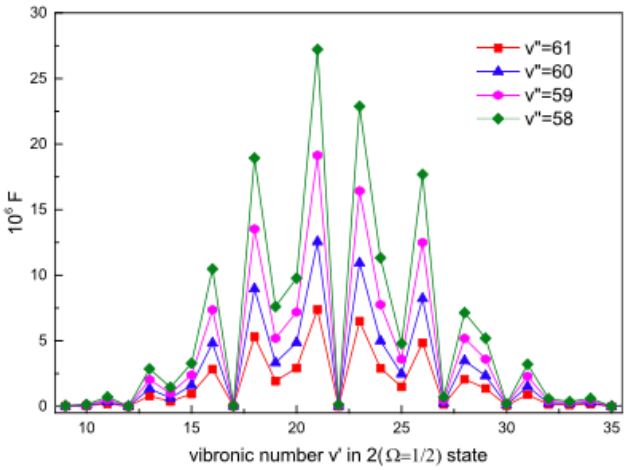


Figure 16: An overview of calculated total F to find the most suitable intermediate state, where the x-axis represents state 2, and the colors show different initial states ($''$). Figure is copied from [24].

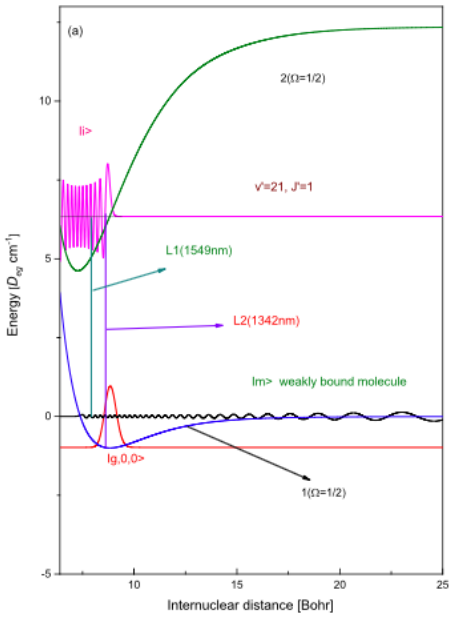


Figure 17: Proposed STIRAP scheme by Chen*et al.* using the state $(2\Omega = 1/2, v' = 21, J' = 1$ as an intermediate state. Figure is copied from [24].

Efficiency of proposed STIRAP schemes

The PEC $2(\Omega = 1/2)$, reflecting an excited molecule with an excitation in the Rb atom is calculated by both Chen *et al.* and Pototschnig *et al.*, and considered to contain suitable intermediate states.

Chen *et al.* did an attempt to predict the efficiency of a full STIRAP round for a $^{84}Sr^{87}Rb$ molecule. Model calculations with parameters chosen based on reasonable assumptions were done to obtain an estimation of the transfer efficiency using the intermediate state ($|2(\Omega = 1/2), v' = 21, J' = 1\rangle$) as shown in figure 17. The proposed pathway was predicted to achieve a round trip efficiency of 60%.

An efficiency calculation is not carried out by the group of Ernst. They used the relation of the Einstein A coefficient with the Rabi frequency to measure the feasibility of potential STIRAP schemes. The Einstein A coefficient is related to the rate of spontaneous emission and absorption of light, and it can be derived from the PECs and FCFs. Although the spontaneous decay from the intermediate state is avoided in STIRAP, spontaneous decay still occurs in the total system in the other states. Therefore the Rabi Frequency is related with the peak intensity of the laser and the Einstein A coefficients by $\Omega \propto \sqrt{I}$ and $I \propto \Gamma_{state}^{-2}$, leading to $I \propto A^{-1}$ [65]. From this relation a equation is set up that expresses the peak intensity of a laserbeam that is needed for a transition with a certain Einstein

A coefficient [12]

$$I^s(mW/mm^2) = \frac{3.7 \cdot 10^2}{A_{v'v''}(s^{-1})(\lambda(nm))^3(t(s))^2}, \tag{40}$$

where I^s is the peak intensity of the applied laser with s being a parameter dependent on the angular momenta J and M. A is the Einstein A coefficient between the two vibrational levels v' and v'', λ is the wavelength of the transition energy, and t is the time duration of the laserpulse. To achieve a high efficiency, the timescale is set to $\Omega_0 \cdot t = 10$ [12]. According to equation 40, and by using assumptions from theoretical research, an Einstein A coefficient of at least 10^{-4} is desired to enable a transition with achievable laser intensities. When the derived Einstein A Coefficients are plotted against transition energies as shown in figure 18, conclusions would be drawn that no STIRAP scheme with a high efficiency would be possible.

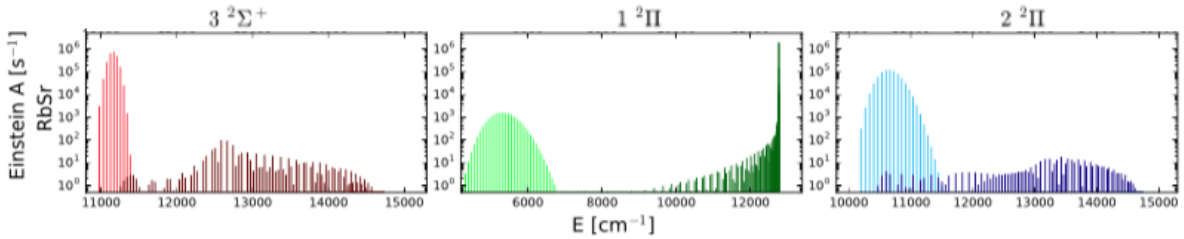


Figure 18: the Einstein A coefficients of the highest vibrational states to the lowest vibrational state through an arbitrary intermediate vibrational level is plotted against transition energies. In these plots the transition energies are shifted by energy differences between of the lowest and highest vibrational states to align excitation and de-excitation to the same value on the x-axis [130]. In this way, overlapping values of excitation and de-excitation show suitable transitions for STIRAP as the transition occurs with the same intermediate state.

A STIRAP scheme through the $1^2\Pi \leftarrow X^2\Sigma$ is assumed to be the most promising as the suitable starting point for a STIRAP scheme [130]. An increase of one magnitude in efficiency is found by using a vibrational level as a starting point that is the second highest of the ground state (v_{max-1}). This level is found to have a better localization and greater overlap with the vibrational levels of the excited states [130].

Although the two methods of efficiency determination quanitatively cannot be compared, the found Einstein A coefficient with values $< 10^{-4}$ by Pototschnig *et al.* can be seen to be in agreement with the predicted efficiency of a round trip STIRAP of 60 % by Chen *et al.*. Because it has to be taken into account that the assumed values of Pototschnig *et al.* are set to achieve very high efficiency. This is not literally stated in the article but can be derived from the recommendations in reference [12]. Besides, the calculations of the Einstein A coefficients do not include SO-coupling, which is probably done for simplicity of the calculations. Including this interaction can change the values slightly.[130] [24].

7 Summary and Outlook

7.1 Summary

The ultracold regime provides an environment that enables the investigation of quantum mechanical behaviour of particles. After the achievement of a BEC, research extends this regime to AK-AKE molecules, which are more complex systems due to the presence of dipole and magnetic moments that bring along long-range interactions [51]. These complex systems give good prospects for quantum devices such as quantum simulators and computers. The RbSr molecule is seen as an anticipated AK-AKE ground state molecule because it has both a dipole moment and a magnetic moment in the ground state [24]. The combination of methods of Feshbach resonances and STIRAP starting from an MI state are proposed to produce a ground state RbSr molecule. The Feshbach resonance associates ultracold Sr and Rb atoms into a weakly-bound RbSr molecule [25]. The weakly-bound RbSr will then to be transfered by STIRAP to the absolute ground state [162].

The use of an MI state, obtained by a 3D optical lattice, is indispensible in this pathway. It promotes the development of the production of the ground state molecule by reduction of inelastic collisions and the control of ultracold atoms in well-defined states [144]. Until now, a lattice mixture have only been obtained for ^{84}Sr-^{87}Rb [10].

So far the FRs method was restricted to only molecules with suitable nuclear magnetic moments. However, technical improvement have enabled the research group of Schreck to observe FRs with very narrow resonance widths for the RbSr molecule [9]. These FRs have been theoretically explained by Brue *et al.* [21] [22]. Three main coupling mechanisms can be used to explain the obeserved FRs. The first is due to the perturbation of the electron distribution of the Rb atoms because of the presence of the Sr atom. The second is due to a polarization of the nuclear spin of the Sr atom by the valence electrons of the Rb atom. The third is due to anisotropic effects of the electron interaction.

To bring the obtained Feshbach molecules to the ground state with the help of STIRAP, detailed knowledge of exact energy levels is needed. In molecules a rich internal structure is seen due to an immense variation of energy levels [7]. Theoretical research is done for RbSr in the ground state and excited state, wich is supported by experimental research using He nano droplets to relax RbSr molecules into the ground state. A proposed STIRAP scheme has been investigated by Chen *et al.* using an $(|2(\Omega = 1/2), v' = 21, J' = 1\rangle)$ intermediate state, with a predicted efficiency of 60% [24]. According to Pototschnig *et al.* a STIRAP scheme through the $1^2\Pi \leftarrow X^2\Sigma$ is assumed to be the most promising, but lacks high efficiency [130]. The group of Schreck performed three types of spectropy experiments of hot and ultracold RbSr molecules to investigate the ground and second excited electronic states of the RbSr molecule. By combining their methods they provided a model representing the complete spectrum of the X$(1)^2\Sigma^+$ ground state of RbSr [27]. This analysis demonstrates a powerful tool to obtain PECs of heavy molecules by inferring molecular spectra and guide future experiments [27].

7.2 Outlook

Weakly-bound states of RbSr

The efficiency of molecule formation depends on the ramp speed and the resonance width as is described in the Landau-Zener model in equation 21. Technical enhancement would give good prospects of higher efficiency and significant Feshbach molecule formation. Nowadays, sophisticated systems have been developed that reduce and correct undesired phenomena, such as optical lattice light shifts in the transition. This has already been shown in the formation of Sr_2, where the correction of the optical lattice light shift led to a significant enhancement in the yield of ultracold Sr_2 molecules [26].

An alternative for creating RbSr molecules into the weakly-bound state would be a double STIRAP pathway, replacing the FR step by STIRAP. An example of this can be found in the formation of Sr_2 ground state molecules [144]. Theoretical calculations have shown this transition to be achievable, but attempts done for $^{84}Sr^{87}Rb$, have not yet been successful [10]. Differences from the Sr_2 situation were found in a much stronger decay rate of the excited state of and a smaller Rabi coupling. Main points of improvement were considered in the isotopologue and compensation of dynamical shift. The isotopologue could greatly effect the efficiency due to differences in transition strength and could provide an increase in Rabi frequency [10]. Furthermore, technical improvement must be made for compensating the dynamical light shift caused by the applied lasers [26].

Ground-state transfer by STIRAP

The choice of an intermediate state for RbSr is according to theoretical research rather restrictive. However prospects for efficient STIRAP in RbSr do not have to be rejected because transition probabilities may be enhanced in presence of Feshbach resonances. This is pointed out in previous research in the formation of ultracold molecules [157] [89] [125]. Furthermore, including SO-coupling in the theoretical calculations can have significant consequences for the vibrational levels [130].

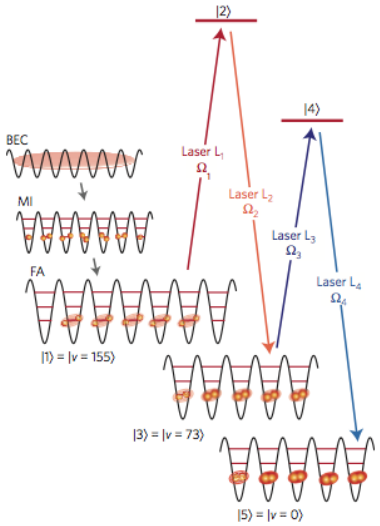


Figure 19: A four laser STIRAP scheme used to for the production of a ground state Cs_2 molecule. Figure is copied from [39].

Another way to overcome small FC overlap could be the use of a four laser transition scheme in which a double STIRAP is applied as is shown in figure 19 for a Cs_2 molecule [39]. Finding such a four laser STIRAP scheme will require more research especially in the vibrational levels to find suitable values in nuclear overlap. New insights in the PEC of ground state and the second excited state of the RbSr molecule found by the group of Schreck will be promising for future experiments [27].

8 Acknowledge

I would like to thank professor Florian Schreck to give me the opportunity to get introduced into the field of research of the creation of ultracold molecules and to give me access to his welcoming and inspiring strontium quantum gas research group. I would like to give a special thanks to Alex Urech who, besides helping me with technical writing, also gave me the mental support and motivation by interesting discussions of the subject. I also like to thank Alessio Ciamei and Lukas Reichsöllner for their time in helping me by their profound and detailed explanations.

References

[1] Aldegunde, J. and Hutson, J. M., arXiv preprint arXiv:1711.09467 (2017).

[2] Alzetta, G., Gozzini, A., Moi, L., and Orriols, G., Il Nuovo Cimento B (1971-1996) **36**, 5 (1976).

[3] Anderson, M. H., Ensher, J. R., Matthews, M. R., Wieman, C. E., Cornell, E. A., *et al.*, Science **269**, 198 (1995).

[4] Anderson, P. W. *et al.*, Science **177**, 393 (1972).

[5] Anglin, J. R. and Ketterle, W., Nature **416**, 211 (2002).

[6] Aoki, T., Yamanaka, Y., Takeuchi, M., Torii, Y., and Sakemi, Y., Physical Review A **87**, 063426 (2013).

[7] Atkins, P. W. and Friedman, R. S., *Molecular quantum mechanics* (Oxford university press, 2011).

[8] Baranov, M., Dalmonte, M., Pupillo, G., and Zoller, P., Chemical Reviews **112**, 5012 (2012).

[9] Barbé, V., Ciamei, A., Pasquiou, B., Reichsöllner, L., Schreck, F., Żuchowski, P. S., and Hutson, J. M., Nature Physics , 1 (2018).

[10] Bayerle, A., *Ultracold strontium and rubidium: Mixtures, quantum gases and molecules* (PhD thesis, Universiteit van Amsterdam, 2017).

[11] Bergmann, K., Theuer, H., and Shore, B., Reviews of Modern Physics **70**, 1003 (1998).

[12] Bergmann, K., Vitanov, N. V., and Shore, B. W., The Journal of Chemical Physics **142**, 170901 (2015).

[13] Bethe, H. A., Physical Review **76**, 38 (1949).

[14] Bethlem, H. L., Berden, G., Crompvoets, F. M., Jongma, R. T., Van Roij, A. J., and Meijer, G., Nature **406**, 491 (2000).

[15] Bize, S., Laurent, P., Abgrall, M., Marion, H., Maksimovic, I., Cacciapuoti, L., Grünert, J., Vian, C., Dos Santos, F. P., Rosenbusch, P., *et al.*, Journal of Physics B: Atomic, molecular and optical physics **38**, S449 (2005).

[16] Bloch, I., Dalibard, J., and Nascimbene, S., Nature Physics **8**, 267 (2012).

[17] Borkowski, M., Żuchowski, P. S., Ciuryło, R., Julienne, P. S., Kędziera, D., Mentel, Ł., Tecmer, P., Münchow, F., Bruni, C., and Görlitz, A., Physical Review A **88**, 052708 (2013).

[18] Born, M. and Fock, V., Zeitschrift für Physik A Hadrons and Nuclei **51**, 165 (1928).

[19] Boyd, M. M., *High Precision Spectroscopy of Strontium in an Optical Lattice: Towards a New Standard for Frequency and Time* (PhD thesis, University of Colorado, 2007).

[20] Breit, G. and Rabi, I., Physical Review **38**, 2082 (1931).

[21] Brue, D. A. and Hutson, J. M., Physical review letters **108**, 043201 (2012).

[22] Brue, D. A. and Hutson, J. M., Physical Review A **87**, 052709 (2013).

[23] Carr, L. D., DeMille, D., Krems, R. V., and Ye, J., New Journal of Physics **11**, 055049 (2009).

[24] Chen, T., Zhu, S., Li, X., Qian, J., and Wang, Y., Physical Review A **89**, 063402 (2014).

[25] Chin, C., Grimm, R., Julienne, P., and Tiesinga, E., Reviews of Modern Physics **82**, 1225 (2010).

[26] Ciamei, A., Bayerle, A., Chen, C.-C., Pasquiou, B., and Schreck, F., Physical Review A **96**, 013406 (2017).

[27] Ciamei, A., Szczepkowski, J., Bayerle, A., Barbé, V., Reichsöllner, L., Tzanova, S. M., Chen, C.-C., Pasquiou, B., Grochola, A., Kowalczyk, P., *et al.*, arXiv preprint arXiv:1806.08586 (2018).

[28] Cirac, J. I. and Zoller, P., Nature Physics **8**, 264 (2012).

[29] Cohen-Tannoudji, C. N., *The Autler-Townes Effect Revisited. In: Chiao R.Y. (eds) Amazing Light* (Springer, New York, NY, 1996) chapter 11.

[30] Comparat, D., Physical Review A **80**, 012106 (2009).

[31] Condon, E. U., Physical Review **32**, 858 (1928).

[32] Courteille, P., Freeland, R., Heinzen, D., Van Abeelen, F., and Verhaar, B., Physical Review Letters **81**, 69 (1998).

[33] Covey, J. P., Moses, S. A., Gärttner, M., Safavi-Naini, A., Miecnikowski, M. T., Fu, Z., Schachenmayer, J., Julienne, P. S., Rey, A. M., Jin, D. S., *et al.*, Nature communications **7** (2016).

[34] Covey, J. P., Moses, S. A., Ye, J., and Jin, D. S., arXiv preprint arXiv:1609.07671 (2016).

[35] Cramer, C. J., *Essentials of computational chemistry: theories and models* (John Wiley & Sons, 2013).

[36] Cubizolles, J., Bourdel, T., Kokkelmans, S., Shlyapnikov, G., and Salomon, C., Physical review letters **91**, 240401 (2003).

[37] Dalgarno, A. and Rudge, M., in *Proceedings of the Royal Society of London A: Mathematical, Physical and Engineering Sciences*, Vol. 286 (The Royal Society, 1965) pp. 519–524.

[38] Danzl, J. G., Haller, E., Gustavsson, M., Mark, M. J., Hart, R., Bouloufa, N., Dulieu, O., Ritsch, H., and Nägerl, H.-C., Science **321**, 1062 (2008).

[39] Danzl, J. G., Mark, M. J., Haller, E., Gustavsson, M., Hart, R., Aldegunde, J., Hutson, J. M., and Nägerl, H.-C., Nature Physics **6**, 265 (2010).

[40] Danzl, J. G., Mark, M. J., Haller, E., Gustavsson, M., Hart, R., Liem, A., Zellmer, H., and Nägerl, H.-C., New Journal of Physics **11**, 055036 (2009).

[41] Davis, K. B., Mewes, M.-O., Andrews, M. R., Van Druten, N., Durfee, D., Kurn, D., and Ketterle, W., Physical review letters **75**, 3969 (1995).

[42] De Miranda, M., Chotia, A., Neyenhuis, B., Wang, D., Quéméner, G., Ospelkaus, S., Bohn, J., Ye, J., and Jin, D., Nature Physics **7**, 502 (2011).

[43] Deiglmayr, J., Grochola, A., Repp, M., Mörtlbauer, K., Glück, C., Lange, J., Dulieu, O., Wester, R., and Weidemüller, M., Physical review letters **101**, 133004 (2008).

[44] Deiglmayr, J., Repp, M., Grochola, A., Mörtlbauer, K., Glück, C., Dulieu, O., Lange, J., Wester, R., and Weidemüller, M., Faraday discussions **142**, 335 (2009).

[45] DeMarco, B. and Jin, D. S., Science **285**, 1703 (1999).

[46] Dieckmann, K., in *Conference on Research Frontiers in Ultra-Cold Atoms*, Vol. 4 (2009) p. 8.

[47] Dirac, P. A. M., in *Proceedings of the Royal Society of London A: Mathematical, Physical and Engineering Sciences*, Vol. 112 (The Royal Society, 1926) pp. 661–677.

[48] Dittmann, P., Pesl, F., Martin, J., Coulston, G., He, G., and Bergmann, K., The Journal of chemical physics **97**, 9472 (1992).

[49] Donley, E. A., Claussen, N. R., Thompson, S. T., and Wieman, C. E., in *Collected Papers Of Carl Wieman* (World Scientific, 2008) pp. 621–625.

[50] Doyle, J., Friedrich, B., Guillet, T., Kim, J., Patterson, D., Weinstein, J., *et al.*, The European Physical Journal D-Atomic, Molecular, Optical and Plasma Physics **7**, 289 (1999).

[51] Doyle, J., Friedrich, B., Krems, R., and Masnou-Seeuws, F., "Quo vadis, cold molecules?" (2004).

[52] Drummond, P., Kheruntsyan, K., Heinzen, D., and Wynar, R., Physical Review A **65**, 063619 (2002).

[53] Dürr, S., Volz, T., Marte, A., and Rempe, G., Physical review letters **92**, 020406 (2004).

[54] Dyke, P., Pollack, S., and Hulet, R., Physical Review A **88**, 023625 (2013).

[55] Einstein, A., *Quantentheorie des einatomigen idealen Gases* (Akademie der Wissenshaften, in Kommission bei W. de Gruyter, 1924).

[56] Endres, M., *Probing correlated quantum many-body systems at the single-particle level* (PhD thesis, Ludwig-Maximilians-Universität München, 2013).

[57] Fano, U., Il Nuovo Cimento (1924-1942) **12**, 154 (1935).

[58] Fano, U., Physical Review **124**, 1866 (1961).

[59] Ferlaino, F., Knoop, S., and Grimm, R., arXiv preprint arXiv:0809.3920 (2008).

[60] Feshbach, H., Annals of Physics **5**, 357 (1958).

[61] Feshbach, H., Annals of Physics **19**, 287 (1962).

[62] Fisher, M. P., Weichman, P. B., Grinstein, G., and Fisher, D. S., Physical Review B **40**, 546 (1989).

[63] Franck, J. and Dymond, E., Transactions of the Faraday Society **21**, 536 (1926).

[64] Gaubatz, U., Rudecki, P., Schiemann, S., and Bergmann, K., The Journal of Chemical Physics **92**, 5363 (1990).

[65] Gerry, C. C. and Knight, P. L., *Introductory Quantum Optics* (Cambridge University Press, Cambridge, 2005).

[66] Goldner, L. S., Gerz, C., Spreeuw, R., Rolston, S., Westbrook, C., Phillips, W. D., Marte, P., and Zoller, P., Physical review letters **72**, 997 (1994).

[67] Gopakumar, G., Abe, M., Hada, M., and Kajita, M., The Journal of Chemical Physics **140**, 224303 (2014).

[68] Gorshkov, A. V., Manmana, S. R., Chen, G., Ye, J., Demler, E., Lukin, M. D., and Rey, A. M., Physical review letters **107**, 115301 (2011).

[69] Greiner, M., Mandel, O., Esslinger, T., Hänsch, T. W., and Bloch, I., nature **415**, 39 (2002).

[70] Greiner, M., Regal, C. A., and Jin, D. S., Nature **426**, 537 (2003).

[71] Grimm, R., Weidemüller, M., and Ovchinnikov, Y. B., Advances in atomic, molecular, and optical physics **42**, 95 (2000).

[72] Guérout, R., Aymar, M., and Dulieu, O., Physical Review A **82**, 042508 (2010).

[73] Guo, M., Zhu, B., Lu, B., Ye, X., Wang, F., Vexiau, R., Bouloufa-Maafa, N., Quéméner, G., Dulieu, O., and Wang, D., Physical review letters **116**, 205303 (2016).

[74] Guttridge, A., Hopkins, S., Kemp, S., Frye, M. D., Hutson, J. M., and Cornish, S. L., arXiv preprint arXiv:1704.03270 (2017).

[75] Hazzard, K. R., Manmana, S. R., Foss-Feig, M., and Rey, A. M., Physical review letters **110**, 075301 (2013).

[76] Herbig, J., Kraemer, T., Mark, M., Weber, T., Chin, C., Nägerl, H.-C., and Grimm, R., Science **301**, 1510 (2003).

[77] Hutson, J. M., New Journal of Physics **9**, 152 (2007).

[78] Hutson, J. M. and Soldan, P., International Reviews in Physical Chemistry **25**, 497 (2006).

[79] Hutzler, N. R., Lu, H.-I., and Doyle, J. M., Chemical reviews **112**, 4803 (2012).

[80] Inouye, S., Andrews, M., Stenger, J., Miesner, H.-J., Stamper-Kurn, D., and Ketterle, W., Nature **392**, 151 (1998).

[81] Ivanov, V. V., Khramov, A., Hansen, A. H., Dowd, W. H., Münchow, F., Jamison, A. O., and Gupta, S., Physical review letters **106**, 153201 (2011).

[82] Jaksch, D., Bruder, C., Cirac, J. I., Gardiner, C. W., and Zoller, P., Physical Review Letters **81**, 3108 (1998).

[83] Jaksch, D., Venturi, V., Cirac, J. I., Williams, C. J., and Zoller, P., Physical review letters **89**, 040402 (2002).

[84] Jaksch, D. and Zoller, P., Annals of physics **315**, 52 (2005).

[85] Javanainen, J. and Mackie, M., Physical Review A **58**, R789 (1998).

[86] Jochim, S., Bartenstein, M., Altmeyer, A., Hendl, G., Chin, C., Denschlag, J. H., and Grimm, R., Physical review letters **91**, 240402 (2003).

[87] Jochim, S., Bartenstein, M., Altmeyer, A., Hendl, G., Riedl, S., Chin, C., Denschlag, J. H., and Grimm, R., Science **302**, 2101 (2003).

[88] Jones, K. M., Tiesinga, E., Lett, P. D., and Julienne, P. S., Reviews of Modern Physics **78**, 483 (2006).

[89] Junker, M., Dries, D., Welford, C., Hitchcock, J., Chen, Y., and Hulet, R., Physical review letters **101**, 060406 (2008).

[90] Kato, T., Journal of the Physical Society of Japan **5**, 435 (1950).

[91] Kerman, A. J., Sage, J. M., Sainis, S., Bergeman, T., and DeMille, D., Physical review letters **92**, 153001 (2004).

[92] Kitching, J., Knappe, S., and Donley, E. A., IEEE Sensors Journal **11**, 1749 (2011).

[93] Kleinert, J., Haimberger, C., Zabawa, P., and Bigelow, N., Physical review letters **99**, 143002 (2007).

[94] Knap, M., Berg, E., Ganahl, M., and Demler, E., Physical Review B **86**, 064501 (2012).

[95] Köhler, T., Góral, K., and Julienne, P. S., Reviews of modern physics **78**, 1311 (2006).

[96] Kostrun, M., Mackie, M., Côté, R., and Javanainen, J., Physical Review A **62**, 063616 (2000).

[97] Kotochigova, S., Tiesinga, E., and Julienne, P. S., Physical Review A **63**, 012517 (2000).

[98] Krems, R., Friedrich, B., and Stwalley, W. C., *Cold molecules: theory, experiment, applications* (CRC press, 2009).

[99] Krois, G., Lackner, F., Pototschnig, J. V., Buchsteiner, T., and Ernst, W. E., Physical Chemistry Chemical Physics **16**, 22373 (2014).

[100] Kuklinski, J., Gaubatz, U., Hioe, F. T., and Bergmann, K., Physical Review A **40**, 6741 (1989).

[101] Külz, M., Keil, M., Kortyna, A., Schellhaa, B., Hauck, J., Bergmann, K., Meyer, W., Weyh, D., *et al.*, Physical Review A **53**, 3324 (1996).

[102] Kuns, K. A., Rey, A. M., and Gorshkov, A. V., Physical Review A **84**, 063639 (2011).

[103] Lackner, F., Krois, G., Buchsteiner, T., Pototschnig, J. V., and Ernst, W. E., Physical review letters **113**, 153001 (2014).

[104] Landau, L., Phys. Z. Sowjetunion **2**, 7 (1932).

[105] Lang, F., Winkler, K., Strauss, C., Grimm, R., and Denschlag, J. H., Physical Review Letters **101**, 133005 (2008).

[106] Lepers, M. and Dulieu, O., arXiv preprint arXiv:1703.02833 (2017).

[107] Marcelis, B., Verhaar, B., and Kokkelmans, S., Physical review letters **100**, 153201 (2008).

[108] Marte, A., Volz, T., Schuster, J., Dürr, S., Rempe, G., Van Kempen, E., and Verhaar, B., Physical Review Letters **89**, 283202 (2002).

[109] Marte, P., Zoller, P., and Hall, J. L., Physical Review A **44**, R4118 (1991).

[110] Messiah, A., *Quantum mechanics* (North-Holland Publishing Company, 1966).

[111] Micheli, A., Brennen, G., and Zoller, P., Nature Physics **2**, 341 (2006).

[112] Mies, F., Tiesinga, E., and Julienne, P. S., Physical Review A **61**, 022721 (2000).

[113] Moerdijk, A., Verhaar, B., and Axelsson, A., Physical Review A **51**, 4852 (1995).

[114] Molony, P. K., Gregory, P. D., Ji, Z., Lu, B., Köppinger, M. P., Le Sueur, C. R., Blackley, C. L., Hutson, J. M., and Cornish, S. L., Physical review letters **113**, 255301 (2014).

[115] Moore, M. and Sadeghpour, H., Physical Review A **67**, 041603 (2003).

[116] Moses, S., Covey, J., Miecnikowski, M., Jin, D., and Ye, J., Nature Physics **13**, 13 (2017).

[117] Moses, S. A., Covey, J. P., Miecnikowski, M. T., Yan, B., Gadway, B., Ye, J., and Jin, D. S., Science **350**, 659 (2015).

[118] Mott, N. F., Massey, H. S. W., *et al.*, *The theory of atomic collisions*, Vol. 35 (Clarendon Press Oxford, 1965).

[119] Nemitz, N., Baumer, F., Münchow, F., Tassy, S., and Görlitz, A., Physical Review A **79**, 061403 (2009).

[120] Ni, K.-K., Ospelkaus, S., De Miranda, M., Pe'Er, A., Neyenhuis, B., Zirbel, J., Kotochigova, S., Julienne, P., Jin, D., and Ye, J., Science **322**, 231 (2008).

[121] Okano, M., Hara, H., Muramatsu, M., Doi, K., Uetake, S., Takasu, Y., and Takahashi, Y., Applied Physics B: Lasers and Optics **98**, 691 (2010).

[122] Oreg, J., Hioe, F., and Eberly, J., Physical Review A **29**, 690 (1984).

[123] Park, J. W., Will, S. A., and Zwierlein, M. W., Physical review letters **114**, 205302 (2015).

[124] Pasquiou, B., Bayerle, A., Tzanova, S. M., Stellmer, S., Szczepkowski, J., Parigger, M., Grimm, R., and Schreck, F., Physical Review A **88**, 023601 (2013).

[125] Pellegrini, P., Gacesa, M., and Côté, R., Physical review letters **101**, 053201 (2008).

[126] Phillips, W. D., Reviews of Modern Physics **70**, 721 (1998).

[127] Pillet, P., Valentin, C., Yuan, R.-L., and Yu, J., Physical Review A **48**, 845 (1993).

[128] Pototschnig, J. V., Krois, G., Lackner, F., and Ernst, W. E., The Journal of Chemical Physics **141**, 234309 (2014).

[129] Pototschnig, J. V., Krois, G., Lackner, F., and Ernst, W. E., Journal of molecular spectroscopy **310**, 126 (2015).

[130] Pototschnig, J. V., Meyer, R., Hauser, A. W., and Ernst, W. E., Physical Review A **95**, 022501 (2017).

[131] Rangwala, S. A., Junglen, T., Rieger, T., Pinkse, P. W., and Rempe, G., Physical Review A **67**, 043406 (2003).

[132] Regal, C. and Jin, D., Advances In Atomic, Molecular, and Optical Physics **54**, 1 (2007).

[133] Regal, C. A., Ticknor, C., Bohn, J. L., and Jin, D. S., Nature **424**, 47 (2003).

[134] Reynolds, M., Shinkoda, I., Cline, R., and Hardy, W., Physical Review B **34**, 4912 (1986).

[135] Roy, R., Shrestha, R., Green, A., Gupta, S., Li, M., Kotochigova, S., Petrov, A., and Yuen, C. H., Physical Review A **94**, 033413 (2016).

[136] Sawyer, B. C., Lev, B. L., Hudson, E. R., Stuhl, B. K., Lara, M., Bohn, J. L., and Ye, J., Physical review letters **98**, 253002 (2007).

[137] Schreck, F., Ferrari, G., Corwin, K., Cubizolles, J., Khaykovich, L., Mewes, M.-O., and Salomon, C., Physical Review A **64**, 011402 (2001).

[138] Shore, B. W., Acta Physica Slovaca **63**, 361 (2013).

[139] Silvera, I. F., American Journal of Physics **65**, 570 (1997).

[140] Sørensen, L. K., Knecht, S., Fleig, T., and Marian, C. M., The Journal of Physical Chemistry A **113**, 12607 (2009).

[141] Steck, D. A., "Rubidium 87 d line data," (2001).

[142] Stein, A., Ivanova, M., Pashov, A., Knöckel, H., and Tiemann, E., The Journal of Chemical Physics **138**, 114306 (2013).

[143] Stellmer, S., *Degenerate quantum gases of strontium* (PhD thesis, University of Innsbruck, 2012).

[144] Stellmer, S., Pasquiou, B., Grimm, R., and Schreck, F., Physical review letters **109**, 115302 (2012).

[145] Stellmer, S., Tey, M. K., Huang, B., Grimm, R., and Schreck, F., Physical review letters **103**, 200401 (2009).

[146] Stoof, H. T. C., Koelman, J., and Verhaar, B., Physical Review B **38**, 4688 (1988).

[147] Strecker, K. E., Partridge, G. B., and Hulet, R. G., Physical review letters **91**, 080406 (2003).

[148] Stwalley, W. C., Physical Review Letters **37**, 1628 (1976).

[149] Sugawa, S., Inaba, K., Taie, S., Yamazaki, R., Yamashita, M., and Takahashi, Y., Nature Physics **7**, 642 (2011).

[150] Szczepkowski, J., Grochola, A., Kowalczyk, P., Dulieu, O., Guérout, R., Żuchowski, P. S., and Jastrzebski, W., Journal of Quantitative Spectroscopy and Radiative Transfer **210**, 217 (2018).

[151] Szymanska, M. H., Góral, K., Köhler, T., and Burnett, K., arXiv preprint cond-mat/0501728 (2005).

[152] Takekoshi, T., Reichsöllner, L., Schindewolf, A., Hutson, J. M., Le Sueur, C. R., Dulieu, O., Ferlaino, F., Grimm, R., and Nägerl, H.-C., Physical review letters **113**, 205301 (2014).

[153] Tassy, S., Nemitz, N., Baumer, F., Höhl, C., Batär, A., and Görlitz, A., Journal of Physics B: Atomic, Molecular and Optical Physics **43**, 205309 (2010).

[154] Taylor, J. R., *Scattering Theory: A Quantum Theory on Nonrelavistic Collisions* (Wiley, 1972).

[155] Tiesinga, E., Verhaar, B., and Stoof, H., Physical Review A **47**, 4114 (1993).

[156] Timmermans, E., Tommasini, P., Hussein, M., and Kerman, A., Physics Reports **315**, 199 (1999).

[157] Tolra, B. L., Hoang, N., T'jampens, B., Vanhaecke, N., Drag, C., Crubellier, A., Comparat, D., and Pillet, P., EPL (Europhysics Letters) **64**, 171 (2003).

[158] Townsend, C., Edwards, N., Cooper, C., Zetie, K., Foot, C., Steane, A., Szriftgiser, P., Perrin, H., and Dalibard, J., Physical Review A **52**, 1423 (1995).

[159] Van Abeelen, F. and Verhaar, B., Physical review letters **83**, 1550 (1999).

[160] Vitanov, N. and Stenholm, S., Physical Review A **55**, 648 (1997).

[161] Vitanov, N. V., Halfmann, T., Shore, B. W., and Bergmann, K., Annual review of physical chemistry **52**, 763 (2001).

[162] Vitanov, N. V., Rangelov, A. A., Shore, B. W., and Bergmann, K., Reviews of Modern Physics **89**, 015006 (2017).

[163] Weinstein, J. D., Guillet, T., Friedrich, B., Doyle, J. M., *et al.*, Nature **395**, 148 (1998).

[164] Winkler, K., Lang, F., Thalhammer, G., vd Straten, P., Grimm, R., and Denschlag, J. H., Physical review letters **98**, 043201 (2007).

[165] Winkler, K., Thalhammer, G., Theis, M., Ritsch, H., Grimm, R., and Denschlag, J. H., Physical review letters **95**, 063202 (2005).

[166] Wynar, R., Freeland, R., Han, D., Ryu, C., and Heinzen, D., Science **287**, 1016 (2000).

[167] Xu, K., Mukaiyama, T., Abo-Shaeer, J., Chin, J. K., Miller, D., and Ketterle, W., Physical review letters **91**, 210402 (2003).

[168] Yao, N. Y., Gorshkov, A. V., Laumann, C. R., Läuchli, A. M., Ye, J., and Lukin, M. D., Physical review letters **110**, 185302 (2013).

[169] Yatsenko, L., Shore, B., and Bergmann, K., Physical Review A **89**, 013831 (2014).

[170] Zahzam, N., Vogt, T., Mudrich, M., Comparat, D., and Pillet, P., Physical review letters **96**, 023202 (2006).

[171] Zener, C., in *Proceedings of the Royal Society of London A: Mathematical, Physical and Engineering Sciences*, Vol. 137 (The Royal Society, 1932) pp. 696–702.

[172] Zhang, J., Van Kempen, E., Bourdel, T., Khaykovich, L., Cubizolles, J., Chevy, F., Teichmann, M., Tarruell, L., Kokkelmans, S., and Salomon, C., Physical Review A **70**, 030702 (2004).

[173] Zhang, P., Sadeghpour, H. R., and Dalgarno, A., The Journal of Chemical Physics **133**, 044306 (2010).

[174] Zhang, X. and Ye, J., National Science Review **3**, 189 (2016).

[175] Zirbel, J., Ni, K.-K., Ospelkaus, S., D'Incao, J., Wieman, C., Ye, J., and Jin, D., Physical review letters **100**, 143201 (2008).

[176] Zirbel, J., Ni, K.-K., Ospelkaus, S., Nicholson, T., Olsen, M., Julienne, P., Wieman, C., Ye, J., and Jin, D., Physical Review A **78**, 013416 (2008).

[177] Żuchowski, P. S., Aldegunde, J., and Hutson, J. M., Physical review letters **105**, 153201 (2010).

[178] Żuchowski, P. S., Guerout, R., and Dulieu, O., Physical Review A **90**, 012507 (2014).

[179] Zwerger, W., Journal of Optics B: Quantum and Semiclassical Optics **5**, S9 (2003).

[180] Zwierlein, M. W., Stan, C. A., Schunck, C. H., Raupach, S. M., Gupta, S., Hadzibabic, Z., and Ketterle, W., Physical review letters **91**, 250401 (2003).